





Cite this: *Environ. Sci.: Nano*, 2021,  
8, 3262

# Cellular response of freshwater algae to halloysite nanotubes: alteration of oxidative stress and membrane function†

Xiaochen Huang, <sup>a</sup> Yichao Huang, <sup>bc</sup> Dali Wang, <sup>d</sup> Mingxian Liu, <sup>\*e</sup>  
Jing Li<sup>\*d</sup> and Da Chen<sup>d</sup>

Halloysite nanotubes (HNTs) are a low-cost clay nanomaterial that has received an increasing amount of attention for applications in various fields. The use of HNT-containing products inevitably leads to their release into aquatic environments. However, the biological effects of HNTs on aquatic organisms remain poorly understood. This study investigated the potential effects of HNTs on model freshwater alga *Chlorella vulgaris* at the tissue, cellular, and subcellular levels and compared the effects with those of HNTs' main constituents: nSiO<sub>2</sub>, nAl<sub>2</sub>O<sub>3</sub>, and a mixture of nSiO<sub>2</sub> and nAl<sub>2</sub>O<sub>3</sub>. The results revealed that these tested nanomaterials inhibited algal growth in a dose-dependent manner and the inhibition capacity followed the trend nAl<sub>2</sub>O<sub>3</sub> > HNTs ≈ nSiO<sub>2</sub> + nAl<sub>2</sub>O<sub>3</sub> > nSiO<sub>2</sub>. However, exposure to HNTs triggered greater levels of reactive oxygen species (ROS) than exposure to the nSiO<sub>2</sub> + nAl<sub>2</sub>O<sub>3</sub> mixture without significantly changing enzyme activity. Surface and ultrastructural observations combined with flow cytometry supported the hypothesis that the nanotubular structure of HNTs impaired membrane integrity and induced overproduction of ROS. A fatty acid (FA) profile analysis suggested that the increase in monounsaturated FAs such as C17:1 and C18:1/n-9 may alter the cell membrane fluidity under HNT exposure. Cell defense to HNTs was mediated by the FA saturation degree or the activity of FA desaturase. This study provides novel insights into the environmental safety of HNTs in aquatic ecosystems.

Received 10th June 2021,  
Accepted 3rd September 2021

DOI: 10.1039/d1en00531f

rsc.li/es-nano

## Environmental significance

Halloysite nanotubes (HNTs), a type of aluminosilicate clay, have brought increasing applications in various fields. However, once HNTs largely released into the aquatic environment, their behavior and even toxicity require to be great concerned. Therefore, the thorough investigation of interactions between HNTs and aquatic organisms is helpful for understanding their environmental risks. This study lies in the exploration of biological effects, at the cellular and subcellular levels, of HNTs on freshwater algae as a model organism. A comparative study with nanosized SiO<sub>2</sub> and Al<sub>2</sub>O<sub>3</sub> was conducted to illustrate whether the toxicity of HNTs resulted from their main constituents or specific nanotubular structure. This study provides novel insights into the environmental safety of HNTs in aquatic ecosystems.

## Introduction

Nanotechnology provides many promising solutions for the improvement of energy storage, biomaterials, cancer therapy,

environmental remediation, and modern vaccine design.<sup>1,2</sup> For example, the use of nanoscale aluminum oxide (nAl<sub>2</sub>O<sub>3</sub>) as a conjugate may benefit the development of cancer therapeutic vaccines.<sup>3</sup> Nanosized silicon oxide (nSiO<sub>2</sub>) shows great potential in papermaking, catalyst supports, and cosmetics.<sup>4</sup> However, the long-term applications of nanotechnology also have environmental concerns due to the release of nanomaterials into the environment and subsequent environmental and health risks.<sup>5,6</sup> Therefore, green and safe-by-design nanomaterials are expected to be developed with increasing demand as alternatives to conventional nanoparticles.

Halloysite nanotubes (HNTs; Al<sub>2</sub>Si<sub>2</sub>O<sub>5</sub>(OH)<sub>4</sub>·nH<sub>2</sub>O) are rolled kaolinite aluminosilicate sheets with inner Al<sub>2</sub>O<sub>3</sub> octahedra and outer SiO<sub>2</sub> tetrahedra. These nanotubular clay

<sup>a</sup> School of Agriculture, Sun Yat-Sen University, Shenzhen 518107, P. R. China<sup>b</sup> Department of Toxicology, School of Public Health, Anhui Medical University, Hefei 230032, China<sup>c</sup> Key Laboratory of Environmental Toxicology of Anhui Higher Education Institutes, Hefei 230032, China<sup>d</sup> Guangdong Key Laboratory of Environmental Pollution and Health, School of Environment, Jinan University, Guangzhou 514443, P. R. China.

E-mail: jli909@163.com

<sup>e</sup> Department of Materials Science and Engineering, Jinan University, Guangzhou 510632, P. R. China. E-mail: liumx@jnu.edu.cn

† Electronic supplementary information (ESI) available. See DOI: 10.1039/d1en00531f

materials are broadly geologically distributed in China, the United States, Australia, and other regions around the world.<sup>7</sup> Approximately 30 000 tons of halloysite minerals are exploited annually for manufacturing into nanotubes.<sup>8</sup> Owing to their abundant reserves in natural environments and low cost (~\$4 per kg), HNTs have received an increasing amount of interest in industrial, environmental, and biomedical fields.<sup>9</sup> For example, HNTs have been applied as a prospective anchor for core-shell metal supports to facilitate heterogeneous catalytic reactions<sup>10</sup> due to their superior surface groups such as outer-surface Si-OH and inner-surface Al-OH groups. HNT-based adsorbents, catalysts, and membranes have also been reported for applications in wastewater remediation and water purification.<sup>11-15</sup> In addition, HNTs have broad application prospects in healthcare, energy storage, cosmetic, biosensor, and feed additive applications.<sup>16-19</sup>

In contrast with the increasing application of HNTs, knowledge of their biological effects and environmental safety remains limited. Available studies on higher plants,<sup>20</sup> *Escherichia coli*,<sup>21</sup> *Caenorhabditis elegans*,<sup>22</sup> zebrafish,<sup>23</sup> and mice<sup>24</sup> have suggested that HNTs' biological effects are highly species- and dose-dependent. For example, the freshwater protozoan *Paramecium caudatum* maintains a higher than 90% survival rate when exposed to 10 mg mL<sup>-1</sup> HNTs,<sup>25</sup> which is ten times the recommended safe dose for cells (1 mg mL<sup>-1</sup>).<sup>26</sup> Up to 25 mg mL<sup>-1</sup> HNTs were reported to not harm the hatchability and morphological development of zebrafish embryos.<sup>23</sup> However, relatively limited data and cross-study variations in biological effects mean that a more thorough elucidation of the environmental safety of HNTs is required.

Algae constitute a major food source to primary consumers in aquatic ecosystems. Compared with zebrafish and zooplankton, algae exhibit more sensitive responses to nanomaterials (e.g., carbon quantum dots<sup>27</sup> and TiO<sub>2</sub> (ref. 28)), making them ideal for evaluating biological responses to emerging nanomaterials.<sup>29-31</sup> Algal cell membranes, as the main target attacked by nanoparticles, subtly reflect biological responses *via* changes to the membrane components (e.g., lipids, saccharides, and proteins).<sup>32</sup> Among these, fatty acids (FAs), as the support for biological growth and metabolic function, have two important implications for the exploration of nanomaterials' biological effects. On the one hand, the variation of FA profiles resulting from nanomaterial exposure can effectively reflect the level of cell membrane permeability and fluidity.<sup>33</sup> Zhang *et al.* reported that exposure to oxidized multiple-wall carbon nanotubes (CNTs) for 8 h significantly altered FA compositions in algae for cellular defense.<sup>31</sup> On the other hand, nanomaterials could also have a commercial impact on algae because several FAs in algae are an important source of nutraceuticals.<sup>34</sup> It is reasonable to believe that the impact of HNTs on valuable nutrients including FAs in algae may affect the food quality of primary producers and subsequently affect overall ecosystem health.

Therefore, in this present study, our specific goals were to: (1) investigate the biological effects of HNTs on freshwater algae (*Chlorella vulgaris*) at the cellular and subcellular levels; and (2) explore whether the unique structure and surface properties of HNTs could lead to biological effects on algae that differ from the outcomes caused by exposure to nSiO<sub>2</sub> and nAl<sub>2</sub>O<sub>3</sub> (the main components of HNTs). This study enables a better understanding of the interactions between HNTs and algae and provides new insights into the potential environmental implications of HNTs in aquatic ecosystems.

## Materials and methods

### Characteristics of nanomaterials

Halloysite nanotubes (HNTs) were obtained from Guangzhou Runwo Materials Technology Co., Ltd. (Guangzhou, China). Nanosized Al<sub>2</sub>O<sub>3</sub> (primary particle size: ~80 nm) and SiO<sub>2</sub> (primary particle size: ~30 nm) were obtained from Macklin Biochemical Technology Co., Ltd. (Shanghai, China). The surface functional groups of the three nanomaterials were determined by Fourier transform infrared (FTIR) spectroscopy (Nicolet iS50, Thermo Scientific, USA).<sup>35</sup> Their morphologies were characterized by scanning electron microscopy (SEM, ULTRA 55, ZEISS, Germany). Their zeta potentials and particle sizes were determined using a Zetasizer (NanoBrook Omni, Brookhaven, New York, USA). The nanomaterial characterization details are summarized in ESI† Texts S1 and S2.

### Evaluation of algal growth

The freshwater alga *Chlorella vulgaris* FACHB-9 was obtained from the Institute of Hydrobiology, Chinese Academy of Science, China. The algae were pre-cultured in a sterile BG-11 medium in an illumination incubator shaker at 25 ± 0.5 °C at a 150 rpm rotation rate, 70% humidity, and a 14 h/10 h light-dark cycle. The exponential stage of algal growth was achieved at ~60 h for further inhibition tests. Algal growth during the pre-cultivation stage was determined by both the cell number and density, measured with a blood counting chamber under an optical microscope (CKX53SF, OLYMPUS, Japan) and a UV-vis spectrophotometer at 680 nm, respectively. According to the correlation between the cell density and number (Fig. S1†), an initial optical density of 0.1 (cell number: 1.1 × 10<sup>6</sup> cells per mL) was determined for algal growth inhibition assays.

The test concentrations of HNTs were selected to be 0.05, 0.1, 0.2, 0.5, 1, 2, 5, and 10 mg mL<sup>-1</sup> based on our previous work.<sup>23</sup> Previous studies have reported that nSiO<sub>2</sub> and nAl<sub>2</sub>O<sub>3</sub> are the main components in raw HNTs, constituting approximately 55% and 32% of HNTs by mass, respectively.<sup>24</sup> Herein, nSiO<sub>2</sub> (0.05, 0.1, 0.2, 0.55, 1, 2, and 5 mg mL<sup>-1</sup>) and nAl<sub>2</sub>O<sub>3</sub> (0.05, 0.1, 0.2, 0.32, 1, 2, and 5 mg mL<sup>-1</sup>) were tested to compare their biological effects with those of HNTs. Suspensions of these three nanomaterials were prepared using sterile BG-11 medium treated with sonication (100 W, 40 kHz, 25 °C) for 30 min, followed by storage at 4 °C. To

investigate the inhibition effects, *C. vulgaris* ( $1.1 \times 10^6$  cells per mL) was exposed to HNTs, nSiO<sub>2</sub>, or nAl<sub>2</sub>O<sub>3</sub> in a 250 mL flask (working volume: 100 mL) for 96 h. Cultures for the 96 h inhibition tests followed the same conditions employed during the pre-culture stage. Algae cultures in the absence of nanomaterials were employed as control groups. The 96 h growth inhibition ratio (%) was calculated as follows:  $(N_0 - N_1)/N_0 \times 100$ , where  $N_0$  and  $N_1$  denote the algal cell numbers at 0 h and 96 h, respectively.<sup>36</sup> The 96 h of 50% effective concentration (EC<sub>50</sub>) was determined based on cell numbers and Probit regression (IBP SPSS package for Windows, version 22.0, IBM Corp., USA).

In addition, based on the percentage of nSiO<sub>2</sub> and nAl<sub>2</sub>O<sub>3</sub> in pristine HNTs,<sup>24</sup> 1 mg mL<sup>-1</sup> HNTs, 0.55 mg mL<sup>-1</sup> nSiO<sub>2</sub>, 0.32 mg mL<sup>-1</sup> nAl<sub>2</sub>O<sub>3</sub>, and a mixture of 0.55 mg mL<sup>-1</sup> nSiO<sub>2</sub> and 0.32 mg mL<sup>-1</sup> nAl<sub>2</sub>O<sub>3</sub> were further selected as exposure concentrations to compare the algal biological response toward HNTs with the responses toward the main HNT components after 96 h exposure. Physical damage, oxidative stress, element release, and adsorption, and FA profiles were determined. The details are summarized in ESI† Texts S3–S7.

### Physical damage and oxidative stress

Algae were collected following 96 h exposure to the test nanomaterials, centrifuged (1500g) at 4 °C for 10 min, and rinsed twice with phosphate buffer solution (PBS, 0.1 M, pH 7.0). Scanning electron microscopy (SEM, ULTRA 55, ZEISS, Germany) and transmission electron microscopy (TEM, Tecnai Spirit, FEI, USA) were employed to investigate algal physical damage.<sup>30</sup> The detailed pretreatment procedures for the SEM and TEM analyses are summarized in the ESI†.

The level of reactive oxygen species (ROS) in the algal cells was determined using a fluorescence spectrophotometer (HITACHI F-4600, Japan). Membrane integrity and mitochondrial membrane potential (MMP) were determined using a flow cytometer (Gallios, Beckman Coulter, USA). The detailed methods of these analyses are shown in ESI† Text S5. The levels of superoxide dismutase (SOD), catalase (CAT), malonaldehyde (MDA), and glutathione (GSH) in the cells were determined using assay kits (Nanjing Jiancheng Bioengineering Institute, China). Enzyme activities were measured with a soluble protein assay kit (Beyotime Biotechnology Co., Ltd., China). Prior to the measurements, treated algal cells were collected by centrifugation (3000g, 5 min) and quickly moved to a liquid nitrogen (−196 °C) tank for 20 min, then thawed at 4 °C. After repeating the freezing and thawing steps four times (~1.5 h/time), crude enzymes were obtained for further index determination. The detailed procedures followed the manufacturer's instructions.

### Determination of FA profiles

The extraction of FAs from algal cells was based on a modified version of a previously reported method.<sup>37</sup> Briefly, 30 mL of algal cell suspension was centrifuged (5000g) to remove the supernatant. Approximately 0.5 mL of algae cell

precipitate was spiked with C17:0 (heptadecanoic acid, Sigma-Aldrich) as an internal standard and extracted with an equal volume of methylbenzene. The mixture was subsequently saponified with 6% (m/v) sodium hydroxide methanolic solution and transmethylated with 10% (v/v) acetylchloride methanolic solution, both under heated conditions. Finally, the fatty acid methyl esters (FAMES) were extracted with *n*-hexane and concentrated. Instrumental analysis of the FAMES was conducted on an Agilent 7890B gas chromatograph coupled with a 5977B MSD detector (Agilent Technologies, USA).<sup>38</sup> Details on the sample preparation and instrumental analysis are summarized in the ESI†.

### Statistical analysis

Experimental data from triplicate treatments were presented as the mean ± standard deviation (SD) and analyzed with a one-way ANOVA to determine significant differences ( $p < 0.05$ ) using SPSS. The relationships between algal cell growth inhibition and enzymes, ROS, or MMP were determined by linear fitting curves (Origin 9, Origin Lab Corp., USA).

## Results and discussion

### Unique functional groups of HNTs and colloidal stability

HNTs possess unique outer and inner structures (Fig. 1A) and contain abundant functional groups and colloidal stability, demonstrating a different behavior to that of nSiO<sub>2</sub> or nAl<sub>2</sub>O<sub>3</sub> particles. For example, the FTIR spectroscopic peaks at 3695 cm<sup>-1</sup> and 3620 cm<sup>-1</sup> correspond to the Al<sub>2</sub>-OH stretching peak and stretching vibrations of the inner surface of the HNTs, respectively (Fig. 1B).<sup>8,39</sup> The peaks at 1092 and 1029 cm<sup>-1</sup> correspond to the stretching vibrations of Si-O-Si groups in HNTs. The peaks representing the stretching vibrations of hydroxyl groups and molecular water are separately located at 1618 cm<sup>-1</sup> for nSiO<sub>2</sub>, 1628 cm<sup>-1</sup> for nAl<sub>2</sub>O<sub>3</sub>, and 1637 cm<sup>-1</sup> for HNTs. A strong peak observed at 910 cm<sup>-1</sup> is attributed to the bending vibration of Al-OH in the HNT spectrum, but this peak is not present in the nAl<sub>2</sub>O<sub>3</sub> spectrum.

The colloidal stability of spheric and aspheric nanomaterials is widely evaluated by dynamic light scattering (DLS). As shown in Fig. 1C and S2†, the hydrodynamic diameters of all the nanomaterials in the algal medium are larger than their individual sizes, indicating that the presence of the algal medium potentially causes particle aggregation. The time-course hydrodynamic diameters of HNTs, nSiO<sub>2</sub>, and nSiO<sub>2</sub> + nAl<sub>2</sub>O<sub>3</sub> in the algal medium suggest the immediate formation of HNTs and nSiO<sub>2</sub> aggregates and the formation of nSiO<sub>2</sub> + nAl<sub>2</sub>O<sub>3</sub> heteroaggregates (Fig. 1C). This is further confirmed by SEM observation (Fig. 2E). Different electrostatic interactions between the nanomaterials and algal cells were also observed between the positively charged nAl<sub>2</sub>O<sub>3</sub> and negatively charged nSiO<sub>2</sub>, HNTs, and the nSiO<sub>2</sub> + nAl<sub>2</sub>O<sub>3</sub> mixture (Fig. S3†). Among these nanomaterials, HNTs exhibit the strongest stability and the lowest zeta potential in

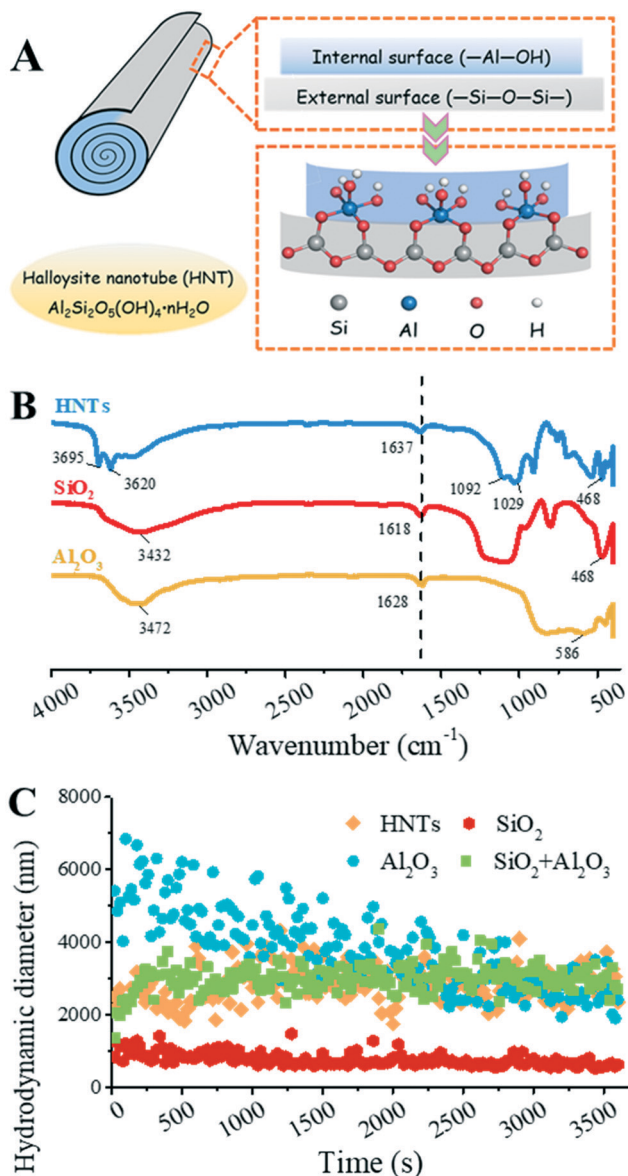


**Fig. 1** Characterization of the tested nanomaterials (A–C). The structure of HNTs (A); the FTIR spectra of HNTs, nSiO<sub>2</sub>, and nAl<sub>2</sub>O<sub>3</sub> (B); and the hydrodynamic diameters (C) following exposure to the tested nanomaterials.

the algal medium. These results demonstrate that HNTs have different structures and chemical properties than nSiO<sub>2</sub>, nAl<sub>2</sub>O<sub>3</sub>, or nSiO<sub>2</sub> + nAl<sub>2</sub>O<sub>3</sub>, which suggests that the biological effects of HNTs likely also differ from those induced by the other nanomaterials.

### HNTs induced lower growth inhibition but stronger oxidative stress

The dose–response relationships of algal exposure to HNTs, nAl<sub>2</sub>O<sub>3</sub>, and nSiO<sub>2</sub> were determined at concentrations ranging from 0 to 10 mg mL<sup>-1</sup> (Fig. S4†). Low doses of HNTs (0–1 mg mL<sup>-1</sup>) for 96 h gradually inhibited algal growth, while increasing the HNT concentration from 1 to 10 mg

mL<sup>-1</sup> enhanced the algal stress responses (Fig. S4A†). The EC<sub>50</sub> of HNTs was determined to be 8.2 mg mL<sup>-1</sup>. In contrast, the calculated 96 h EC<sub>50</sub> values of nAl<sub>2</sub>O<sub>3</sub> and nSiO<sub>2</sub> are 0.35 and 12.5 mg mL<sup>-1</sup>, respectively. Interestingly, growth stimulation by nSiO<sub>2</sub> was also observed at low doses of 0.05–1 mg mL<sup>-1</sup> (Fig. S4B†), likely due to the stress-response hormesis caused by the nanomaterials.<sup>40</sup> A comparison of the inhibitory effect of HNTs (1 mg mL<sup>-1</sup>) on algal growth and that of the other tested nanomaterials reveals the following pattern: nSiO<sub>2</sub> < nSiO<sub>2</sub> + nAl<sub>2</sub>O<sub>3</sub> ≈ HNTs < nAl<sub>2</sub>O<sub>3</sub> (Fig. 3A). HNTs exhibit greater algal inhibition than nSiO<sub>2</sub>, likely due to nSiO<sub>2</sub>-induced hormesis or the adverse effects of HNT impurities on algae.<sup>25,41</sup> Unexpectedly, nSiO<sub>2</sub> + nAl<sub>2</sub>O<sub>3</sub> exhibited a similar inhibitory effect to that of HNTs, which was probably caused by the formation of abundant nSiO<sub>2</sub> + nAl<sub>2</sub>O<sub>3</sub> aggregates in the algal medium (Fig. 1C and 2E) reducing the physical contact of nSiO<sub>2</sub>/nAl<sub>2</sub>O<sub>3</sub> with algal cells. Reporting a similar phenomenon, Zhao *et al.* showed that the formation of graphene oxide (GO)–Al<sub>2</sub>O<sub>3</sub> heteroaggregates mitigated GO's algal toxicity.<sup>42</sup> In contrast, the nSiO<sub>2</sub> + nAl<sub>2</sub>O<sub>3</sub> aggregates were unlikely to form under HNT exposure due to the separation of nSiO<sub>2</sub> and nAl<sub>2</sub>O<sub>3</sub> in the inner and outer surface of the pristine HNTs. Therefore, HNTs and nSiO<sub>2</sub> + nAl<sub>2</sub>O<sub>3</sub> may inhibit algal growth *via* different mechanisms, although they exhibit similar inhibition ratios.

SEM observation reveals distinct interactions between the tested nanomaterials and the algal cells (Fig. 2A–E). HNT exposure results in the attachment of the nanomaterials on the algal cell surfaces (Fig. 2B), probably due to the occurrence of Ca bridging in the algal medium. Furthermore, due to their unique nanotubular structure and electrostatic functions, HNTs could facilitate the direct puncture of cell walls with their tips. A similar behavior has been reported for CNT exposure.<sup>31</sup> The uptake of HNTs by other cells such as MCF-7 cells, A549 cells, and lung cells has also been reported.<sup>43–45</sup> The nAl<sub>2</sub>O<sub>3</sub> nanomaterials were highly coated on wrinkled algal cells during nAl<sub>2</sub>O<sub>3</sub> exposure (Fig. 2D), suggesting that physical damage is caused by electrostatic attraction.<sup>42</sup> In the presence of both nSiO<sub>2</sub> and nAl<sub>2</sub>O<sub>3</sub>, the greater negative charges of nSiO<sub>2</sub> compared to that of the algae increase the opportunity for nAl<sub>2</sub>O<sub>3</sub> to interact with nSiO<sub>2</sub> rather than with the algal cells (Fig. 2E). Thus, it is reasonable to believe that the heteroaggregation of nSiO<sub>2</sub> and nAl<sub>2</sub>O<sub>3</sub> impedes the direct contact of Al<sub>2</sub>O<sub>3</sub> with the algae, resulting in lower growth inhibition than exposure to nAl<sub>2</sub>O<sub>3</sub> by itself (Fig. 3A). The representative TEM images further confirm the differing algal responses to the different nanomaterials at the ultrastructural level (Fig. 2H–L). Exposure to HNTs damaged the algal cell walls and membranes but cellular organelles such as chloroplasts remained intact (Fig. 2I). Exposure to nAl<sub>2</sub>O<sub>3</sub> or nSiO<sub>2</sub> + nAl<sub>2</sub>O<sub>3</sub> induced severe cellular damage, such as plasmolysis (red two-way arrow), reduced plastoglobuli, and blurred thylakoids (Fig. 2K and L).

The determination of algal cell membrane integrity reveals that HNTs damaged the membranes of a greater proportion

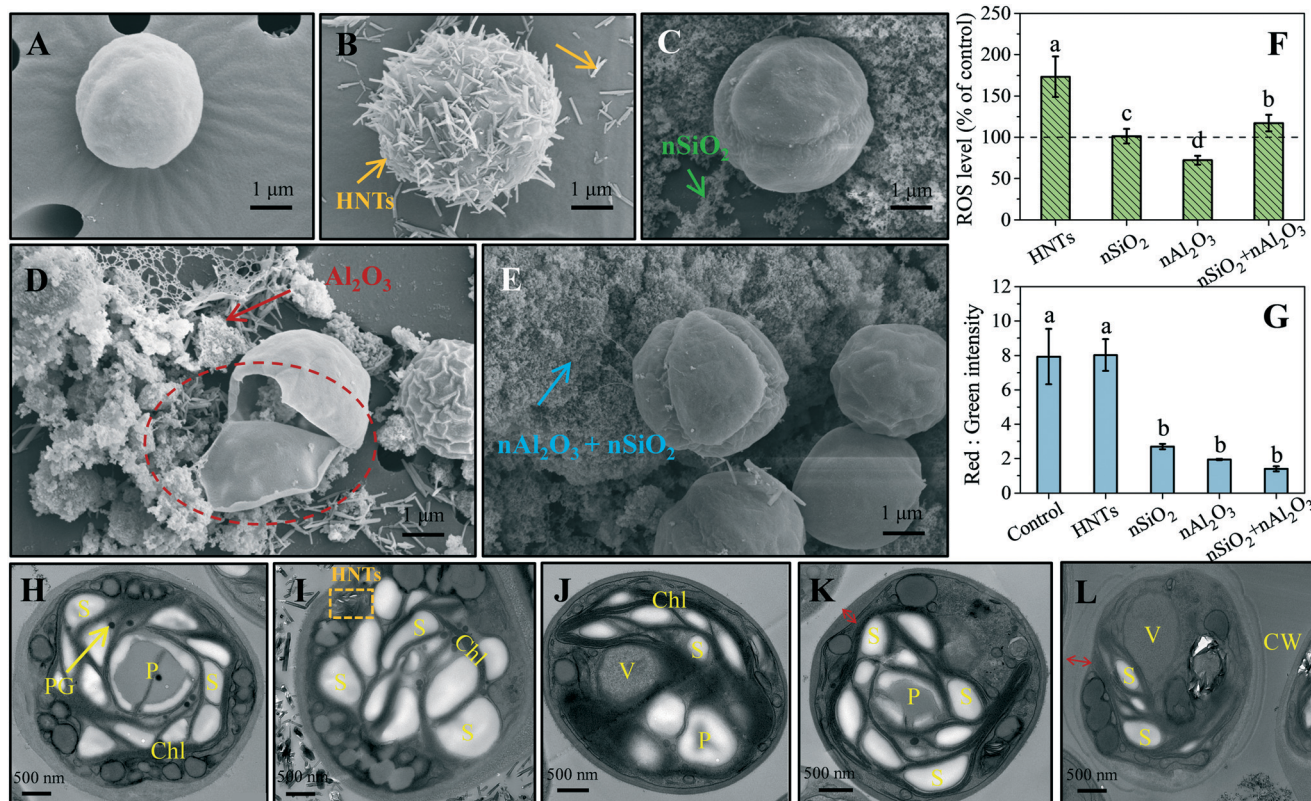


Fig. 2 SEM (A–E) and TEM (H–L) observations, ROS levels (F), and red to green fluorescence intensity ratios (G) of algae after 96 h exposure to nanomaterials. The lowercase letters represent significant differences in ROS or red to green fluorescence intensity ratios among the five treatments.

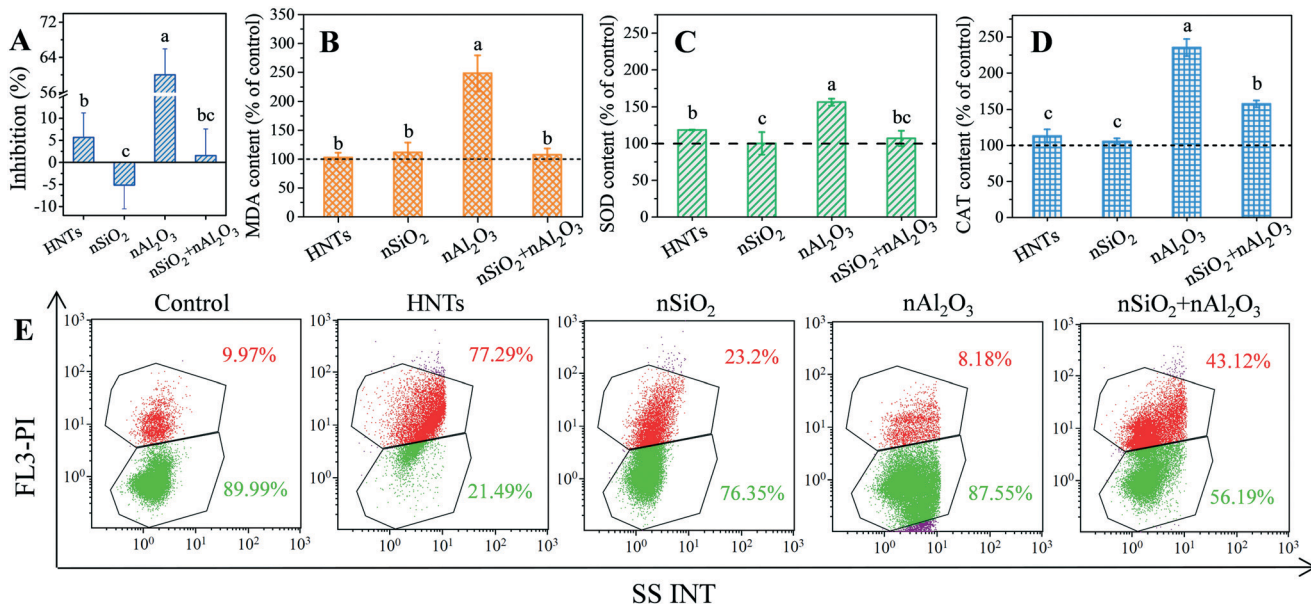


Fig. 3 The growth inhibition (A), relative content of MDA (B), SOD activity (C), and CAT activity (D), and the representative images of membrane damage (E) under exposure to HNTs, nSiO<sub>2</sub>, nAl<sub>2</sub>O<sub>3</sub>, and nSiO<sub>2</sub> + nAl<sub>2</sub>O<sub>3</sub> for 96 h. The lowercase letters represent significant differences in growth inhibition and MDA, SOD, and CAT activity among the four nanomaterial treatments. The green and red regions shown in (E) represent intact and damaged cells.

of algal cells compared to the other nanomaterial exposure treatments (Fig. 3E). The nanotubular structure of HNTs

potentially easily triggers plasma membrane damage *via* penetration and/or energy-dependent endocytosis.<sup>46</sup>

Exposure to nSiO<sub>2</sub> damaged the membranes and blurred organelles (*i.e.*, starch grana and vacuole) of the algal cells. Interestingly, while nAl<sub>2</sub>O<sub>3</sub> exposure significantly inhibited algal growth, it resulted in the lowest ratio of membrane damage, suggesting that the transport of nAl<sub>2</sub>O<sub>3</sub> to algal cells may be through the release of Al ions rather than the endocytosis of nanoscale Al particles. Indeed, our experiments confirmed that 0.23% Al was released from nAl<sub>2</sub>O<sub>3</sub> (Fig. S5 and S6<sup>†</sup>), likely contributing to approximately 76.5% of its algal growth inhibition. In addition, the effect of nutrition depletion by nanomaterial-induced algal growth inhibition can be ruled out (Fig. S7 and S8<sup>†</sup>) based on our results summarized in ESI<sup>†</sup> Text S8.

In addition to physical damage, HNT exposure triggered greater levels of ROS than any other nanomaterial treatment (Fig. 2F), suggesting that the balance of cellular homeostasis was disrupted and that the biological functions of the cell membranes were impaired. Induced oxidative stress due to overproduction of ROS is considered to be one of the main toxicity mechanisms of nanomaterials.<sup>47</sup> When the ROS level exceeds the antioxidant defense capacity (*i.e.*, SOD and CAT), lipid peroxidation further occurs in cells.<sup>48</sup> However, the MDA content in the HNT-treated algae did not differ significantly from that of the control treatment (Fig. 3B). The low MDA and high ROS levels indicate that there are other antioxidants or pathways involved in cellular protection from excessive ROS during HNT treatment. Indeed, elevated SOD and CAT levels were found in the algae treated with HNTs compared with the control treatment (Fig. 3C and D). SOD and CAT, as the main antioxidant enzymes, are activated to respectively scavenge O<sub>2</sub><sup>•-</sup> and H<sub>2</sub>O<sub>2</sub> for cellular defense against nanomaterial-induced inhibition.<sup>49</sup> These findings suggested that cellular protection was activated following HNT exposure. Mitotoxicity is another pathway that can cause oxidative stress,<sup>50</sup> but HNT exposure did not significantly affect the MMP levels (Fig. 2G). Therefore, the HNTs maintain mitochondrial membrane integrity without inducing mitotoxicity.

In contrast, nAl<sub>2</sub>O<sub>3</sub> triggered severe oxidative stress in the algal cells, as reflected by the higher levels of SOD activity, CAT activity, MDA content, and GSH content as well as the lower MMP compared to the other treated algal cells (Fig. 2G, 3B–D, and S9B<sup>†</sup>). However, the intracellular ROS levels caused by nAl<sub>2</sub>O<sub>3</sub> treatment were significantly lower than those of the other treatments (Fig. 2F). Exposure to nSiO<sub>2</sub> + nAl<sub>2</sub>O<sub>3</sub> resulted in a significant increase in CAT activity compared with HNT exposure (Fig. 3D), suggesting that nSiO<sub>2</sub> + nAl<sub>2</sub>O<sub>3</sub> exposure triggers the overproduction of H<sub>2</sub>O<sub>2</sub> radicals, which are scavenged by CAT.<sup>51</sup> Furthermore, correlation analysis reveals that nanomaterial-induced algal growth inhibition is positively correlated with antioxidants (Fig. S10<sup>†</sup>), while the ROS levels are strongly related to the percentage of membrane-damaged algal cells (Fig. S11F<sup>†</sup>). Therefore, we reasonably believe that both physical contact and oxidative stress are responsible for HNT-induced membrane damage.

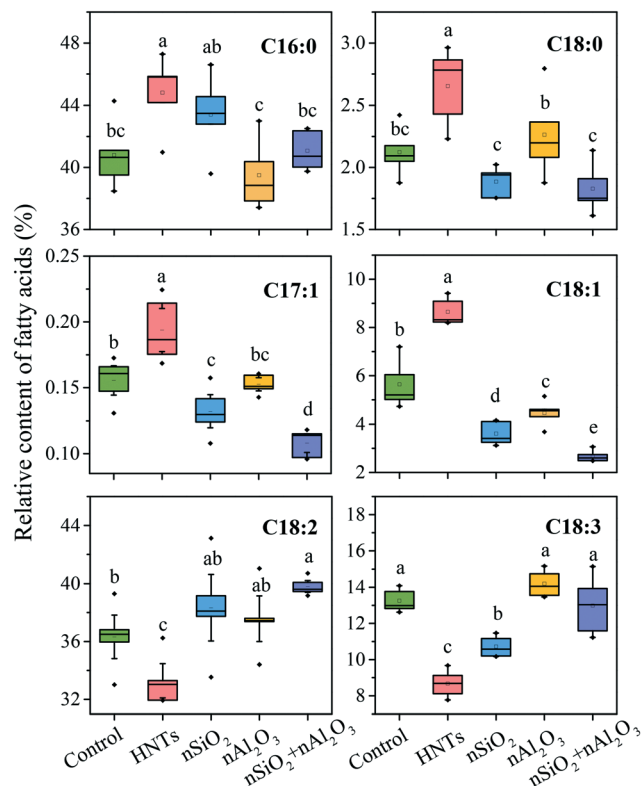
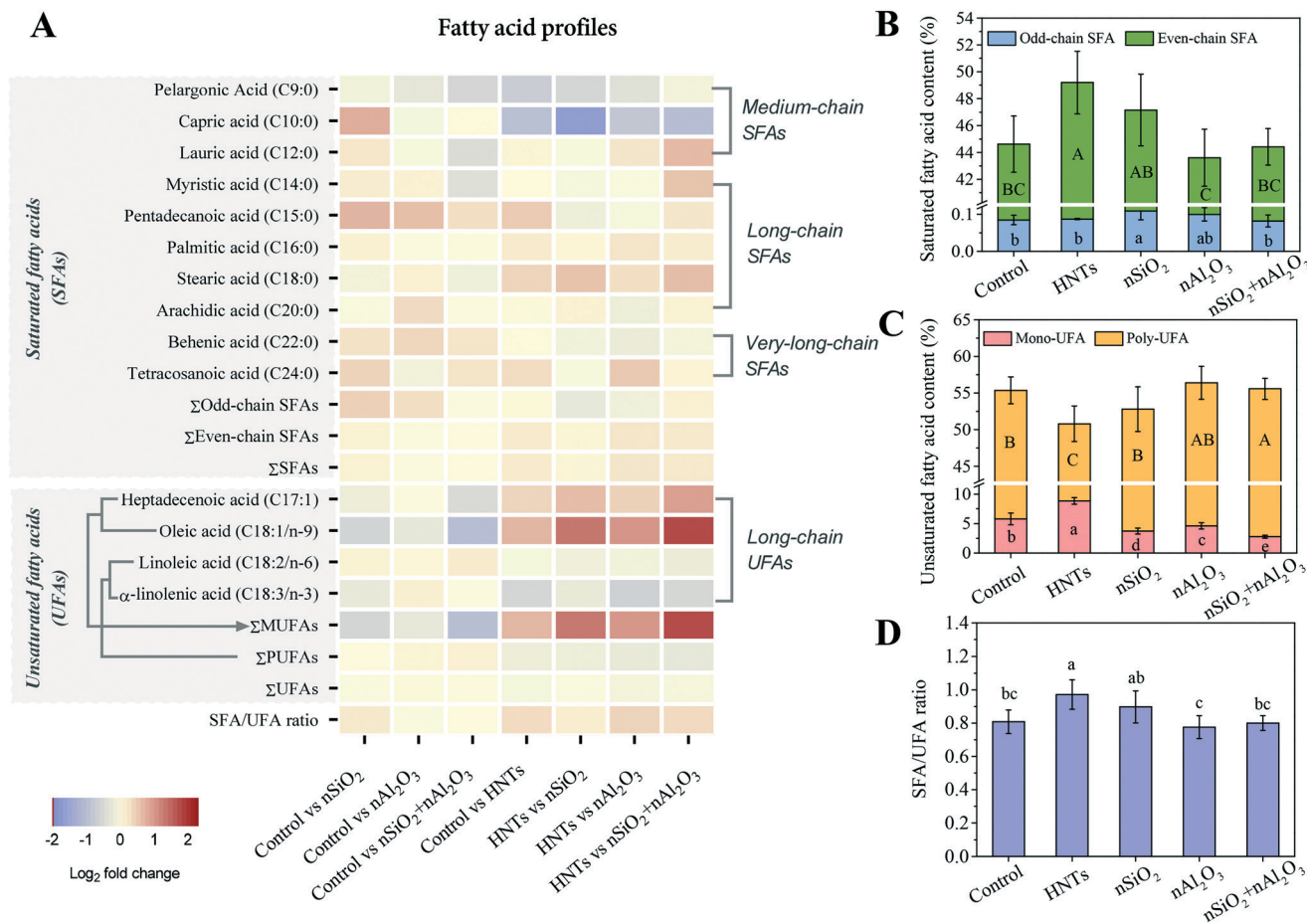


Fig. 4 The change in the relative content of SFAs and UFAs under exposure to HNTs, nSiO<sub>2</sub>, nAl<sub>2</sub>O<sub>3</sub>, and nSiO<sub>2</sub> + nAl<sub>2</sub>O<sub>3</sub>. The boxes suggest the median interquartile range and the bars denote the concentration range. The lowercase letters represent significant differences in the data among the five treatments.

#### HNTs altered the FA compositions of algal cells

In addition to the antioxidants discussed in the previous sections, several FAs were also involved in cellular defense against HNT exposure (Fig. 4 and S12<sup>†</sup>). Fifteen FAs, including ten saturated fatty acids (SFAs) and four unsaturated fatty acids (UFAs), were identified in *C. vulgaris*. Their main components are palmitic acid (C16:0), linoleic acid (C18:2/n-6),  $\alpha$ -linolenic acid (C18:3/n-3), oleic acid (C18:1/n-9), and stearic acid (C18:0). This FA profile is in good agreement with previous reports on FA compositions in the same species.<sup>37</sup> In general, phytotoxicity triggered by nanomaterials can occur at the tissue, cellular, and even molecular levels.<sup>52</sup> Both metabolomic and transcriptomic analyses have revealed that FA metabolism is an important pathway that is likely involved in algal responses to nanomaterials.<sup>34,40,53–55</sup> In agreement with this study, Zou *et al.* found that single-layer MoS<sub>2</sub> nanosheets incubated with humic acid significantly reduced algal growth inhibition but induced the overproduction of ROS, indicating that FAs may play an important role in cellular defense to oxidative stress.<sup>54</sup>

In this work, HNT exposure significantly boosted the relative content of SFAs but reduced that of polyunsaturated fatty acids (PUFAs) and total UFAs (Fig. 5B and C). This behavior is regarded as one of the cellular responses of algae to nanomaterials.<sup>34</sup> Mortimer *et al.* attributed the



**Fig. 5** Difference analysis heatmap of the five treatments (A), composition of SFAs (B) and UFAs (C), and the SFA/UFA ratio (D). The lowercase and uppercase letters represent significant differences in the data among the five treatments.

decreased total concentration of UFAs in nanoscale CuO-exposed protozoan cells to the cells' adaptive regulation to stress.<sup>33</sup> Specifically, PUFAs are involved in cell structural functions and are susceptible to pollutants.<sup>32,56,57</sup> The sharp decrease in C18:2/n-6 and C18:3/n-3 under HNT exposure, as well as the drastic elevation of C16:0 and C18:0, is potentially due to the physical destruction of membrane integrity by the nanotubular structure (Fig. 3E). A negative correlation between PUFAs and ROS levels, although not statistically significant ( $p = 0.08$ ; Fig. S13<sup>†</sup>), possibly suggests the susceptibility of PUFAs to ROS attack.<sup>32</sup>

The change in the FA profile under HNT exposure differed from that of the other nanomaterial treatments (Fig. 4 and S12<sup>†</sup>). Combined with the differential analysis shown in Fig. 5A, it can be concluded that C10:0, sum of monounsaturated fatty acids (ΣMUFAs), C17:1, and C18:1/n-9 are the most sensitive to HNT exposure, rendering them candidate biomarkers for investigating lipid-related adverse effects upon exposure to HNTs. Additionally, a significant increase in the SFA/UFA ratio (*i.e.*, from 0.81 to 0.97) was observed in the algal cells under HNT exposure (Fig. 5D), but not for any of the other treatments. The SFA/UFA ratio is of great importance for the maintenance of membrane

function.<sup>32</sup> A disrupted SFA/UFA ratio in nanomaterial-exposed plants indicates the alteration of membrane fluidity and stability. This has been observed for plant cells under exposure to CNTs, Ag nanoparticles, and nano CuO.<sup>32,56,58</sup> Our data suggest that algal cell defense to HNTs is potentially mediated by the FA saturation degree or the activity of FA desaturase.<sup>59</sup> Consequently, as part of their defense mechanisms, algae may restrict exogenous substances like HNTs from entering the cells by decreasing cell membrane fluidity.

Overall, compared with nSiO<sub>2</sub>, nAl<sub>2</sub>O<sub>3</sub>, and nSiO<sub>2</sub> + nAl<sub>2</sub>O<sub>3</sub> exposure, HNT exposure exhibits different biological impacts on algae, including growth inhibition, oxidative stress, and membrane function, due to the unique physicochemical properties of HNTs. The nanotubular structure of HNTs does not induce severe growth inhibition, but the HNTs may enter algal cells *via* endocytosis and puncturing, which destroys their cell membrane integrity and alters their FA composition. HNTs potentially induce cellular protection biological responses in algae by increasing the FA desaturation degree. This is a different behavior than that of algae exposed to nSiO<sub>2</sub>, nAl<sub>2</sub>O<sub>3</sub>, or nSiO<sub>2</sub> + nAl<sub>2</sub>O<sub>3</sub>, in which cellular protection likely occurs *via* the mediation of antioxidases.

## Environmental implications

Along with HNTs' industrial applications, its environmental and ecological safety warrants better elucidations. Our results suggest that HNTs are relatively safe but that the stimulation of oxidative stress in algal cells requires their use to be dialectically considered in aquatic ecosystems. Specifically, the high levels of oxidative stress induced by HNTs played a dominant role in their nanotoxicity. However, this is potentially beneficial for algae-based biofuel production *via* lipid accumulation in algal cells under HNT exposure. In addition, the change in the FA profile caused by HNT exposure may have specific environmental implications in terms of their use as a food source and for green bioenergy generation.

HNT exposure may impact the competitiveness of algae as a nutritious food source. Algae-derived PUFAs (mainly microalgae) are nutritious and profitable molecules due to their ability to provide essential FAs for cardiovascular, neurological, and ocular health.<sup>60</sup> Linoleic acid (C18:2/n-6), an essential PUFA precursor, cannot be synthesized *de novo* in the human body, so it is an important dietary supplement. The potential applications of  $\gamma$ -linolenic acid (C18:3/n-9, GLA) are mainly infant formulas for full-term infants and nutritional supplements. Our data reveal that HNT exposure could significantly reduce PUFAs. Thus, this exposure may result in a decline in the nutritional value of *C. vulgaris* to primary consumers and possibly other organisms in aquatic ecosystems.

In contrast, HNT exposure may be beneficial for the application of algae as a commercial feedstock for the production of sustainable biofuels.<sup>61,62</sup> Whether algae can be considered a commercial feedstock depends on their lipid productivity and quality.<sup>63</sup> Lipid quality is highly correlated to FA profile. For example, the European Biodiesel Standard EN14212 requires the linolenic acid concentration in biodiesel to be less than 12% to maintain the balance of oxidative stability.<sup>64</sup> The relative content of  $\alpha$ -linolenic acid in the control treatment exceeded this biodiesel standard (13.3%), while HNT-treated algae demonstrated a reduced  $\alpha$ -linolenic acid proportion of 8.7%. In addition, biodiesel containing high levels of oleic acid has a lower cold filter plugging point, making it more suitable for cold weather use.<sup>65</sup> Consequently, the increase in the C18:1/n-9 concentration under HNT exposure, as shown in Fig. 4, is very promising. Thus, the changing FA profiles of algae under HNT exposure could potentially meet the quality requirements of biodiesel feedstock. Therefore, the presence of HNTs in aquatic ecosystems should be dialectically considered.

## Author contributions

Xiaochen Huang: conceptualization, formal analysis, funding acquisition, investigation, project administration, writing – original draft, writing – review & editing. Yichao Huang: formal analysis, funding acquisition, software, writing –

review & editing. Dali Wang: resources. Mingxian Liu: conceptualization, funding acquisition, supervision. Jing Li: supervision. Da Chen: conceptualization, funding acquisition, resources, supervision, writing – review & editing.

## Conflicts of interest

The authors declare that they have no competing financial interests.

## Acknowledgements

This work was financially supported by the National Natural Science Foundation of China (No. 42007285, 52073121, and 82173484), the Guangdong Natural Science Foundation (2019A1515011509), the Guangdong (China) Innovative and Entrepreneurial Research Team Program (No. 2016ZT06N258), and the Fundamental Research Funds for the Central Universities (No. 21619102 and 2021qntd19).

## References

- 1 M. D. Shin, S. Shukla, Y. H. Chung, V. Beiss, S. K. Chan, O. A. Ortega-Rivera, D. M. Wirth, A. Chen, M. Sack, J. K. Pokorski and N. F. Steinmetz, COVID-19 vaccine development and a potential nanomaterial path forward, *Nat. Nanotechnol.*, 2020, **15**, 645–655.
- 2 E. Maine, V. J. Thomas, M. Bliemel, A. Murira and J. Utterback, The emergence of the nanobiotechnology industry, *Nat. Nanotechnol.*, 2014, **9**, 2–5.
- 3 H. Li, Y. Li, J. Jiao and H. M. Hu, Alpha-alumina nanoparticles induce efficient autophagy-dependent cross-presentation and potent antitumour response, *Nat. Nanotechnol.*, 2011, **6**, 645–650.
- 4 Z. Chen, H. Meng, G. Xing, H. Yuan, F. Zhao, R. Liu, X. Chang, X. Gao, T. Wang, G. Jia, C. Ye, Z. Chai and Y. Zhao, Age-related differences in pulmonary and cardiovascular responses to SiO<sub>2</sub> nanoparticle inhalation: nanotoxicity has susceptible population, *Environ. Sci. Technol.*, 2008, **42**, 8985–8992.
- 5 C. Ma, L. Chen, C. Cao and X. Li, Nanoparticle-induced unusual melting and solidification behaviours of metals, *Nat. Commun.*, 2017, **8**, 1–7.
- 6 Y. Li, S. Yu, Q. Wu, M. Tang, Y. Pu and D. Wang, Chronic Al<sub>2</sub>O<sub>3</sub>-nanoparticle exposure causes neurotoxic effects on locomotion behaviors by inducing severe ROS production and disruption of ROS defense mechanisms in nematode *Caenorhabditis elegans*, *J. Hazard. Mater.*, 2012, **219**, 221–230.
- 7 Y. Lvov and E. Abdullayev, Functional polymer-clay nanotube composites with sustained release of chemical agents, *Prog. Polym. Sci.*, 2013, **38**, 1690–1719.
- 8 L. Yu, H. Wang, Y. Zhang, B. Zhang and J. Liu, Recent advances in halloysite nanotube derived composites for water treatment, *Environ. Sci.: Nano*, 2016, **3**, 28–44.
- 9 G. Lazzara, G. Cavallaro, A. Panchal, R. Fakhrullin, A. Stavitskaya, V. Vinokurov and Y. Lvov, An assembly of



- organic-inorganic composites using halloysite clay nanotubes, *Curr. Opin. Colloid Interface Sci.*, 2018, **35**, 42–50.
- 10 L. Kang, L. Han, J. He, H. Li, T. Yan, G. Chen, J. Zhang, L. Shi and D. Zhang, Improved NO<sub>x</sub> Reduction in the Presence of SO<sub>2</sub> by Using Fe<sub>2</sub>O<sub>3</sub>-Promoted Halloysite-Supported CeO<sub>2</sub>-WO<sub>3</sub> Catalysts, *Environ. Sci. Technol.*, 2018, **53**, 938–945.
  - 11 T. Zhou, C. Li, H. Jin, Y. Lian and W. Han, Effective adsorption/reduction of Cr (VI) oxyanion by halloysite@ polyaniline hybrid nanotubes, *ACS Appl. Mater. Interfaces*, 2017, **9**, 6030–6043.
  - 12 K. Zhu, Y. Duan, F. Wang, P. Gao, H. Jia, C. Ma and C. Wang, Silane-modified halloysite/Fe<sub>3</sub>O<sub>4</sub> nanocomposites: simultaneous removal of Cr(VI) and Sb(V) and positive effects of Cr(VI) on Sb(V) adsorption, *Chem. Eng. J.*, 2017, **311**, 236–246.
  - 13 M. Massaro, C. G. Colletti, G. Lazzara, S. Guernelli, R. Noto and S. Riela, Synthesis and characterization of halloysite-cyclodextrin nanosponges for enhanced dyes adsorption, *ACS Sustainable Chem. Eng.*, 2017, **5**, 3346–3352.
  - 14 M. Ghanbari, D. Emadzadeh, W. J. Lau, H. Riazi, D. Almasi and A. F. Ismail, Minimizing structural parameter of thin film composite forward osmosis membranes using polysulfone/halloysite nanotubes as membrane substrates, *Desalination*, 2016, **377**, 152–162.
  - 15 L. Zhu, H. Wang, J. Bai, J. Liu and Y. Zhang, A porous graphene composite membrane intercalated by halloysite nanotubes for efficient dye desalination, *Desalination*, 2017, **420**, 145–157.
  - 16 G. Y. Jia, Z. X. Huang, Y. L. Zhang, Z. Q. Hao and Y. L. Tian, Ultrasensitive plasmonic biosensors based on halloysite nanotubes/MoS<sub>2</sub>/black phosphorus hybrid architectures, *J. Mater. Chem. C*, 2019, **7**, 3843–3851.
  - 17 Y. Lvov, W. Wang, L. Zhang and R. Fakhrullin, Halloysite clay nanotubes for loading and sustained release of functional compounds, *Adv. Mater.*, 2016, **28**, 1227–1250.
  - 18 W. Liang, Y. Wu, H. Sun, Z. Zhu, P. Chen, B. Yang and A. Li, Halloysite clay nanotubes based phase change material composites with excellent thermal stability for energy saving and storage, *RSC Adv.*, 2016, **6**, 19669–19675.
  - 19 A. Panchal, G. Fakhrullina, R. Fakhrullin and Y. Lvov, Self-assembly of clay nanotubes on hair surface for medical and cosmetic formulations, *Nanoscale*, 2018, **10**, 18205–18216.
  - 20 L. Bellani, L. Giorgetti, S. Riela, G. Lazzara, A. Scialabba and M. Massaro, Ecotoxicity of halloysite nanotube-supported palladium nanoparticles in *Raphanus sativus* L, *Environ. Toxicol. Chem.*, 2016, **35**, 2503–2510.
  - 21 A. A. Taylor, G. M. Aron, G. W. Beall, N. Dharmasiri, Y. Zhang and R. J. McLean, Carbon and clay nanoparticles induce minimal stress responses in gram negative bacteria and eukaryotic fish cells, *Environ. Toxicol.*, 2014, **29**, 961–968.
  - 22 G. I. Fakhrullina, F. S. Akhatova, Y. M. Lvov and R. F. Fakhrullin, Toxicity of halloysite clay nanotubes in vivo: a *Caenorhabditis elegans* study, *Environ. Sci.: Nano*, 2015, **2**, 54–59.
  - 23 Z. Long, Y. P. Wu, H. Y. Gao, J. Zhang, X. Ou, R. R. He and M. Liu, In vitro and in vivo toxicity evaluation of halloysite nanotubes, *J. Mater. Chem. B*, 2018, **6**, 7204–7216.
  - 24 X. Wang, J. Gong, R. Rong, Z. Gui, T. Hu and X. Xu, Halloysite nanotubes-induced Al accumulation and fibrotic response in lung of mice after 30-day repeated oral administration, *J. Agric. Food Chem.*, 2018, **66**, 2925–2933.
  - 25 M. Kryuchkova, A. Danilushkina, Y. Lvov and R. Fakhrullin, Evaluation of toxicity of nanoclays and graphene oxide in vivo: a *Paramecium caudatum* study, *Environ. Sci.: Nano*, 2016, **3**, 442–452.
  - 26 F. R. Ahmed, M. H. Shoaib, M. Azhar, S. H. Um, R. I. Yousuf, S. Hashmi and A. Dar, In-vitro assessment of cytotoxicity of halloysite nanotubes against HepG2, HCT116 and human peripheral blood lymphocytes, *Colloids Surf., B*, 2015, **135**, 50–55.
  - 27 K. Yao, X. Lv, G. Zheng, Z. Chen, Y. Jiang, X. Zhu, Z. Wang and Z. Cai, Effects of carbon quantum dots on aquatic environments: comparison of toxicity to organisms at different trophic levels, *Environ. Sci. Technol.*, 2018, **52**, 14445–14451.
  - 28 S. Hall, T. Bradley, J. T. Moore, T. Kuykindall and L. Minella, Acute and chronic toxicity of nano-scale TiO<sub>2</sub> particles to freshwater fish, cladocerans, and green algae, and effects of organic and inorganic substrate on TiO<sub>2</sub> toxicity, *Nanotoxicology*, 2009, **3**, 91–97.
  - 29 C. Zhang, X. Huang, Y. Chu, N. Ren and S.-H. Ho, An overlooked effect induced by surface modification: different molecular response of *Chlorella pyrenoidosa* to graphitized and oxidized nanodiamonds, *Environ. Sci.: Nano*, 2020, **7**, 2302–2312.
  - 30 X. Huang, S. Zhu, H. Zhang, Y. Huang, X. Wang, Y. Wang and D. Chen, Biochar nanoparticles induced distinct biological effects on freshwater algae via oxidative stress, membrane damage, and nutrient depletion, *ACS Sustainable Chem. Eng.*, 2021, **9**, 10761–10770.
  - 31 L. Zhang, C. Lei, K. Yang, J. C. White and D. Lin, Cellular response of *Chlorella pyrenoidosa* to oxidized multi-walled carbon nanotubes, *Environ. Sci.: Nano*, 2018, **5**, 2415–2425.
  - 32 J. Yuan, A. He, S. Huang, J. Hua and G. D. Sheng, Internalization and phytotoxic effects of CuO nanoparticles in *Arabidopsis thaliana* as revealed by fatty acid profiles, *Environ. Sci. Technol.*, 2016, **50**, 10437–10447.
  - 33 M. Mortimer, K. Kasemets, M. Vodovnik, R. Marinšek-Logar and A. Kahru, Exposure to CuO nanoparticles changes the fatty acid composition of protozoa *Tetrahymena thermophile*, *Environ. Sci. Technol.*, 2011, **45**, 6617–6624.
  - 34 E. Kadar, P. Rooks, C. Lakey and D. A. White, The effect of engineered iron nanoparticles on growth and metabolic status of marine microalgae cultures, *Sci. Total Environ.*, 2012, **439**, 8–17.
  - 35 S. Zhu, X. Huang, X. Yang, P. Peng, Z. Li and C. Jin, Enhanced transformation of Cr(VI) by heterocyclic-N within nitrogen-doped biochar: impact of surface modulatory persistent free radicals (PFRs), *Environ. Sci. Technol.*, 2020, **54**, 8123–8132.

- 36 J. Zhao, X. Cao, Z. Wang, Y. Dai and B. Xing, Mechanistic understanding toward the toxicity of graphene-family materials to freshwater algae, *Water Res.*, 2017, **111**, 18–27.
- 37 I. Lang, L. Hodac, T. Friedl and I. Feussner, Fatty acid profiles and their distribution patterns in microalgae: a comprehensive analysis of more than 2000 strains from the SAG culture collection, *BMC Plant Biol.*, 2011, **11**, 124.
- 38 Y. Huang, F. Sun, H. Tan, Y. Deng, Z. Sun, H. Chen, J. Li and D. Chen, DEHP and DINP induce tissue-and gender-specific disturbances in fatty acid and lipidomic profiles in neonatal mice: a comparative study, *Environ. Sci. Technol.*, 2019, **53**, 12812–12822.
- 39 G. Karunakaran, R. Suriyaprabha, V. Rajendran and N. Kannan, Toxicity evaluation based on particle size, contact angle and zeta potential of SiO<sub>2</sub> and Al<sub>2</sub>O<sub>3</sub> on the growth of green algae, *Adv. Nano Res.*, 2015, **3**, 243.
- 40 Y. Tong, A. Feng, X. Hou, Q. Zhou and X. Hu, Nanoholes regulate the phytotoxicity of single-layer molybdenum disulfide, *Environ. Sci. Technol.*, 2019, **53**, 13938–13948.
- 41 H. J. Choi, T. J. Stazak and C. D. Montemagno, Surface-dependent cytotoxicity on bacteria as a model for environmental stress of halloysite nanotubes, *J. Nanopart. Res.*, 2013, **15**, 2008.
- 42 J. Zhao, Y. Dai, Z. Wang, W. Ren, Y. Wei, X. Cao and B. Xing, Toxicity of GO to freshwater algae in the presence of Al<sub>2</sub>O<sub>3</sub> particles with different morphologies: importance of heteroaggregation, *Environ. Sci. Technol.*, 2018, **52**, 13448–13456.
- 43 Y. P. Wu, J. Yang, H. Y. Gao, Y. Shen, L. Jiang, C. Zhou, Y. F. Li, R. R. He and M. Liu, Folate-conjugated halloysite nanotubes, an efficient drug carrier, deliver doxorubicin for targeted therapy of breast cancer, *ACS Appl. Nano Mater.*, 2018, **1**, 595–608.
- 44 E. Rozhina, A. Panchal, F. Akhatova, Y. Lvov and R. Fakhrullin, Cytocompatibility and cellular uptake of alkylsilane-modified hydrophobic halloysite nanotubes, *Appl. Clay Sci.*, 2020, **185**, 105371.
- 45 R. Rong, Y. Zhang, Y. Zhang, Y. Hu, W. Yang, X. Hu, L. Wen and Q. Zhang, Inhibition of inhaled halloysite nanotube toxicity by trehalose through enhanced autophagic clearance of p62, *Nanotoxicology*, 2019, **13**, 354–368.
- 46 X. Shi, A. von Dem Bussche, R. H. Hurt, A. B. Kane and H. Gao, Cell entry of one-dimensional nanomaterials occurs by tip recognition and rotation, *Nat. Nanotechnol.*, 2011, **6**, 714–719.
- 47 P. P. Fu, Q. Xia, H. M. Hwang, P. C. Ray and H. Yu, Mechanisms of nanotoxicity: generation of reactive oxygen species, *J. Food Drug Anal.*, 2014, **22**, 64–75.
- 48 M. Schieber and N. S. Chandel, ROS function in redox signaling and oxidative stress, *Curr. Biol.*, 2014, **24**, R453–R462.
- 49 E. D. Harris, Regulation of antioxidant enzymes, *FASEB J.*, 1992, **6**(9), 2675–2683.
- 50 M. C. Stensberg, R. Madangopal, G. Yale, Q. Wei, H. Ochoa-Acuña, A. Wei, E. S. Mclamore, J. Rickus, D. M. Porterfield and M. S. Sepúlveda, Silver nanoparticle-specific mitotoxicity in *Daphnia magna*, *Nanotoxicology*, 2014, **8**, 833–842.
- 51 F. Li, Z. Liang, X. Zheng, W. Zhao, M. Wu and Z. Wang, Toxicity of nano-TiO<sub>2</sub> on algae and the site of reactive oxygen species production, *Aquat. Toxicol.*, 2015, **158**, 1–13.
- 52 W. Kang, X. Li, A. Sun, F. Yu and X. Hu, Study of the persistence of the phytotoxicity induced by graphene oxide quantum dots and of the specific molecular mechanisms by integrating omics and regular analyses, *Environ. Sci. Technol.*, 2019, **53**, 3791–3801.
- 53 X. Hu, S. Ouyang, L. Mu, J. An and Q. Zhou, Effects of graphene oxide and oxidized carbon nanotubes on the cellular division, microstructure, uptake, oxidative stress, and metabolic profiles, *Environ. Sci. Technol.*, 2015, **49**, 10825–10833.
- 54 W. Zou, Q. Zhou, X. Zhang and X. Hu, Environmental transformations and algal toxicity of single-layer molybdenum disulfide regulated by humic acid, *Environ. Sci. Technol.*, 2018, **52**, 2638–2648.
- 55 N. S. Taylor, R. Merrifield, T. D. Williams, J. K. Chipman, J. R. Lead and M. R. Viant, Molecular toxicity of cerium oxide nanoparticles to the freshwater alga *Chlamydomonas reinhardtii* is associated with supra-environmental exposure concentrations, *Nanotoxicology*, 2016, **10**, 32–41.
- 56 M. B. Tayemeh, M. Esmailbeigi, I. Shirdel, H. S. Joo, S. A. Johari, A. Banan, H. Nourani, H. Mashhadi, M. J. Jami and M. Tabarrok, Perturbation of fatty acid composition, pigments, and growth indices of *Chlorella vulgaris* in response to silver ions and nanoparticles: a new holistic understanding of hidden ecotoxicological aspect of pollutants, *Chemosphere*, 2020, **238**, 124576.
- 57 Q. Xiong, L. X. Hu, Y. S. Liu, T. T. Wang and G. G. Ying, New insight into the toxic effects of chloramphenicol and roxithromycin to algae using FTIR spectroscopy, *Aquat. Toxicol.*, 2019, **207**, 197–207.
- 58 M. Rui, C. Ma, J. C. White, Y. Hao, Y. Wang, X. Tang, J. Yang, F. Jiang, A. Ali, Y. Rui, W. Cao, G. Chen and B. Xing, Metal oxide nanoparticles alter peanut (*Arachis hypogaea* L.) physiological response and reduce nutritional quality: a life cycle study, *Environ. Sci.: Nano*, 2018, **5**, 2088–2102.
- 59 M. Rui, C. Ma, X. Tang, J. Yang, F. Jiang, Y. Pan, Z. Xiang, Y. Hao, Y. Rui, W. Cao and B. Xing, Phytotoxicity of silver nanoparticles to peanut (*Arachis hypogaea* L.): physiological responses and food safety, *ACS Sustainable Chem. Eng.*, 2017, **5**, 6557–6567.
- 60 P. Spolaore, C. Joannis-Cassan, E. Duran and A. Isambert, Commercial applications of microalgae, *J. Biosci. Bioeng.*, 2006, **101**, 87–96.
- 61 X. Huang, S. Bai, Z. Liu, T. Hasunuma, A. Kondo and S. H. Ho, Fermentation of pigment-extracted microalgal residue using yeast cell-surface display: direct high-density ethanol production with competitive life cycle impacts, *Green Chem.*, 2020, **22**, 153–162.
- 62 M. Y. Menetrez, An overview of algae biofuel production and potential environmental impact, *Environ. Sci. Technol.*, 2012, **46**, 7073–7085.

- 63 V. Ördög, W. A. Stirk, P. Bálint, A. O. Aremu, A. Okem, C. Lovász, Z. Molnár and J. van Staden, Effect of temperature and nitrogen concentration on lipid productivity and fatty acid composition in three *Chlorella* strains, *Algal Res.*, 2016, **16**, 141–149.
- 64 G. Knothe, Analyzing biodiesel: standards and other methods, *J. Am. Oil Chem. Soc.*, 2006, **83**, 823–833.
- 65 S. Stournas, E. Lois and A. Serdari, Effects of fatty acid derivatives on the ignition quality and cold flow of diesel fuel, *J. Am. Oil Chem. Soc.*, 1995, **72**, 433–437.

## Supporting Information

### **Cellular Response of Freshwater Algae to Halloysite Nanotubes: Alteration of Oxidative Stress and Membrane Function**

Xiaochen Huang,<sup>a</sup> Yichao Huang,<sup>b,c</sup> Dali Wang,<sup>d</sup> Mingxian Liu<sup>e,\*</sup>, Jing Li,<sup>d,\*</sup> and Da Chen<sup>d</sup>

<sup>a</sup> *School of Agriculture, Sun Yat-Sen University, Shenzhen 518107, P. R. China*

<sup>b</sup> *Department of Toxicology, School of Public Health, Anhui Medical University, Hefei 230032, China*

<sup>c</sup> *Key Laboratory of Environmental Toxicology of Anhui Higher Education Institutes, Hefei 230032, China*

<sup>d</sup> *Guangdong Key Laboratory of Environmental Pollution and Health, School of Environment, Jinan University, Guangzhou 514443, P. R. China*

<sup>e</sup> *Department of Materials Science and Engineering, Jinan University, Guangzhou 510632, P. R. China*

\*Corresponding authors: *Mingxian Liu*. E-mail: [liumx@jnu.edu.cn](mailto:liumx@jnu.edu.cn), *Jing Li*. E-mail: [jli909@163.com](mailto:jli909@163.com)

## ■ METHODS AND MATERIALS

### **Text S1. FTIR determination**

Briefly, the halloysite nanotubes (HNTs), nanosized SiO<sub>2</sub> (nSiO<sub>2</sub>), nanosized Al<sub>2</sub>O<sub>3</sub> (nAl<sub>2</sub>O<sub>3</sub>), and nSiO<sub>2</sub>+nAl<sub>2</sub>O<sub>3</sub> mixture were ground with infrared quality KBr (w/w, 1:100), vacuum-pressed and measured with the range of 400-4000 cm<sup>-1</sup>. 16 cycles were co-added with a resolution of 2 cm<sup>-1</sup> to enhance signal to noise ratio.

### **Text S2. Zeta potential and particle size**

The suspension of tested nanomaterials were individually prepared in the BG-11 medium and treated with sonication (100 W, 40 kHz, 25 °C) for 30 min. The final concentrations of HNTs, nSiO<sub>2</sub>, and nAl<sub>2</sub>O<sub>3</sub> were 1 mg/mL, 0.55 mg/mL, and 0.32 mg/mL, respectively. The 0.55 mg/mL nSiO<sub>2</sub> and 0.32 mg/mL nAl<sub>2</sub>O<sub>3</sub> were mixed and suspended under sonication treatment and quickly moved in the cuvette for measurements of hydrodynamic diameters using the Zetasizer. The hydrodynamic diameters of nanomaterials were recorded at 0-30 min.

### **Text S3. SEM observation**

The surface morphology of tested nanomaterials, algal cells, and their interactions were determined using SEM (ULTRA 55, ZEISS, Germany). Briefly, the nanomaterials were prepared with absolute ethanol and treated with sonication for 2 h. The interactions between algal cells and nanomaterials were observed after 96-h exposure. Prior to the SEM observations, the samples were rinsed thrice with PBS (0.1 M, pH 7.0), filtered with membrane, freeze-dried, and gold-coated.

#### **Text S4. TEM observation**

The algal cells exposed to nanomaterials were centrifuged (1500 g, 10 min) and fixed with 2.5% glutaraldehyde (v/v) at 4 °C for overnight. Prior to fix with 1% osmium tetroxide (v/v) for 1-2 h, samples were thoroughly rinsed thrice (15 min/time) with PBS (0.1 M, pH 7.0). After repeatedly washing step by PBS, the samples were dehydrated with the increasing concentrations of ethanol (30%, 50%, 70%, 80%, 90%, 95%, and 100%) in sequence for 15-20 min and 100% acetone for 20 min. Epoxy resin and 100% acetone mixed at 1:1 and 3:1 (v/v) were subsequently used for permeation and embedding. Ultramicrotome (EM UC7, Leica, Germany) was employed to obtain ultra-thin algal samples (70-90 nm), which were then strained with lead citrate and uranyl acetate for 5-10 min. The ultrastructure of algal cells were mounted on copper grids and observed using a TEM (Tecnai Spirit, FEI, USA).

#### **Text S5. Determination of reactive oxygen species (ROS), membrane integrity, and mitochondrial membrane potential (MMP)**

In brief, treated algal cells were centrifuged and then rinsed thrice with PBS (0.1 M, pH 7.0) to resuspend in the PBS solution. For ROS detection, the centrifuged cell pellets were stained with 2',7'-dichlorodihydrofluorescein diacetate (DCFH-DA) in the dark for 15 min and measured fluorescence intensity at 488 nm excitation and 525 nm emission with a fluorescence spectrophotometer (HITACHI F-4600, Japan). Propidium iodide (PI, 1 mg/mL) was used to stain with algal cells in the dark for 15 min to determine membrane integrity using flow cytometer (Gallios, Beckman coulter, USA) at 488 nm excitation and 620 nm emission with a FL3 detector. The JC-1 strained algal cells incubated in the

dark for 15 min were employed to determine MMP. The excitation wavelength for MMP detection was 488 nm, measuring with FL1 detector (green fluorescence) at 520 nm and FL2 detector (red fluorescence) at 580 nm. The loss of MMP was quantified according to ratio value of red to green fluorescence intensity. At least 10000 algal cells were collected and analyzed for each replicate.

### **Text S6. Adsorption of Nutrients and Release of Al and Si**

The adsorption of nutrients by nanomaterials were determined according to the method by Zhao et al.<sup>1</sup> Briefly, HNTs, nSiO<sub>2</sub>, nAl<sub>2</sub>O<sub>3</sub>, and nSiO<sub>2</sub>+nAl<sub>2</sub>O<sub>3</sub> were individually prepared with sterile ultrapure water, added in algal medium, stirred with shaker (150 rpm) at 25 °C for 96 h. The solution was filtered through a 0.22- $\mu$ m membrane filter to obtain the supernatants. The microelements (B, Co, Cu, Zn, Mn, and Fe) and macroelements (Ca, Mg, K, and P) in the supernatants were determined using inductively coupled plasma optical emission spectrometry (ICP-OES, iCAP 7000 Series, Thermo Scientific, USA). The sterile supernatants were applied to cultivate algae for 96 h. Cell numbers were counted to investigate the effects of nutrient removal on algal growth.

To determine the release of Al and Si during treatments, the suspension of HNTs, nSiO<sub>2</sub>, nAl<sub>2</sub>O<sub>3</sub>, or nSiO<sub>2</sub>+nAl<sub>2</sub>O<sub>3</sub> was sonicated for 30 min and then stirred (150 rpm) at 25 °C for 96 h. The suspension was collected every 24 h and filtered through 0.22- $\mu$ m membrane. Concentrations of Al and Si were determined using ICP-OES. To investigate the toxicities of Si or Al ions to algae, Na<sub>2</sub>SiO<sub>3</sub>·9H<sub>2</sub>O (1.2, 23.5, and 48.2 mg/L) and Al(NO<sub>3</sub>)<sub>3</sub>·9H<sub>2</sub>O (0.06, 0.34, and 0.86 mg/L) were separately added in sterile medium to cultivate algae for 96 h.

### **Text S7. Pretreatment for fatty acid (FA) analysis**

An aliquot of 500  $\mu$ L methylbenzene and 20  $\mu$ L C17:0 (1 mg/mL) were added in sequence and

blended by Vortex oscillator (9454FIALUS, Fisher Scientific, USA). The samples were added with 2 mL NaOH-methanol solution (3:50, m/V), heated in water bath (80 °C) for 15 min for saponification. Subsequently, the extract of FAs was treated with acetylchloride-methanol solution (1:10, V/V) at 80 °C for another 15 min for transmethylation. 1 mL K<sub>2</sub>CO<sub>3</sub> and 1 mL *n*-hexane were added sequentially to extract the methyl esters prior to analysis by Gas Chromatography-Mass Spectrometry (GC-MS).

GC separation was achieved using a J&W DB-23 column (60 m × 250 μm × 0.25 μm, Agilent Technologies, USA). Detection used 5977B MSD detector (Agilent Technologies, USA) under electron impact (EI) ionization source followed our previous method.<sup>2</sup> Samples (1 μL) were injected with a split ratio of 20:1 at 250 °C. Helium was used as the carrier gas at a flow rate of 1.2 mL/min. GC oven programs are set as follows: 50 °C for 1 min, a linear ramp to 175 °C at 25 °C/min and held for 2 min, linear ramp to 230 °C at 3 °C/min and held for 5 min. MS ion source was set at 300 °C. The MS detector was operated in the selected ion monitoring (SIM) mode and detailed parameters have been previously summarized.<sup>2</sup> The FAME peaks were identified and quantified according to FAME standard mixture GLC-463 (Nu-Chek, USA) using MassHunter software (Agilent Technologies). Each FA was quantified as their relative weight percentage to the total FAME.

## ■ RESULTS AND DISCUSSION

### **Text S8. Ions release and adsorption depended on media and nanomaterials**

Nanomaterials have ability to release their dissolved ions and absorb ions existed in aqueous phase, depending on nanomaterials' species and cultivation media. These properties could further have impacts on algal biological responses. The 96-h cell number of algae after nutrients removal by four



tested nanomaterials (Fig. S7) suggested that there were no significant differences in cell number between the control and any four treatments, although several nutrients were significantly reduced (Fig. S8). Hoecke et al. also ruled out the hypothesis that CeO<sub>2</sub> nanoparticles induced nutrient depletion was responsible for the toxicity to *Pseudokirchneriella subcapitata* in the presence of OECD medium.<sup>3</sup> In addition, although previous work reported that dissolved ions released from both metallic nanoparticles and HNTs was the predominant contribution to toxicity,<sup>4,5</sup> our study revealed that only 0.23% Al released from nAl<sub>2</sub>O<sub>3</sub> (Figs. S5 and S6). It is worth noting that 0.74 mg/L of Al ions (corresponding to 0.07% Al ions release in Al<sub>2</sub>O<sub>3</sub> NPs) could induce 45.9% growth inhibition, accounting for 76.5% of total growth inhibition. Thus, the mass release of Al from Al<sub>2</sub>O<sub>3</sub> NPs could be the main toxic mechanism to algae. Different biological responses between HNTs and nSiO<sub>2</sub>+nAl<sub>2</sub>O<sub>3</sub> were not attributed to the released ions.

## REFERENCES:

1. J. Zhao, X. Cao, Z. Wang, Y. Dai and B. Xing, Mechanistic understanding toward the toxicity of graphene-family materials to freshwater algae, *Water Res.*, 2017, **111**: 18-27.
2. Y. Huang, F. Sun, H. Tan, Y. Deng, Z. Sun, H. Chen, J. Li and D. Chen, DEHP and DINP induce tissue-and gender-specific disturbances in fatty acid and lipidomic profiles in neonatal mice: a comparative study, *Environ. Sci. Technol.*, 2019, **53**, 12812-12822.
3. K. V. Hoecke, J. T. Quik, J. Mankiewicz-Boczek, K. A. D. Schamphelaere, A. Elsaesser, P. V. D. Meeren, C. Barnes, G. McKerr, C. V. Howard, D. V. D Meent, K. Rydzyński, K. A. Dawson, A. Salvati, A. Lesniak, I. Lynch, G. Silversmit, B. D. Samber, L. Vincze and K. Rydzyński, Fate and effects of CeO<sub>2</sub> nanoparticles in aquatic ecotoxicity tests, *Environ. Sci. Technol.* 2009, **43**, 4537-

4546.

4. F. Chen, Z. Xiao, L. Yue, J. Wang, Y. Feng, X. Zhu, Z. Wang and Xing, B, Algae response to engineered nanoparticles: current understanding, mechanisms and implications, *Environ. Sci.: Nano*. 2019, **6**, 1026-1042.
5. X. Wang, J. Gong, Z. Gui, T. Hu and X. Xu, Halloysite nanotubes-induced Al accumulation and oxidative damage in liver of mice after 30-day repeated oral administration, *Environ. Toxicol.* 2018, **33**, 623-630.

■ Tables

Table S1 Composition of BG-11 medium used for the culture of *Chlorella vulgaris*.

	Components	Concentration (g/L)
Regular solution	NaNO <sub>3</sub>	1.5
	K <sub>2</sub> HPO <sub>4</sub>	0.04
	MgSO <sub>4</sub> ·7H <sub>2</sub> O	0.075
	Citric acid	0.006
	CaCl <sub>2</sub> ·2H <sub>2</sub> O	0.036
	Na <sub>2</sub> CO <sub>3</sub>	0.02
	Ferric ammonium citrate	0.006
	Na <sub>2</sub> ·EDTA·2H <sub>2</sub> O	0.001
-----		
A5	H <sub>3</sub> BO <sub>3</sub>	2.86
(trace metal mix solution, *10 <sup>-3</sup> )	MnCl <sub>2</sub> ·4H <sub>2</sub> O	1.81
	ZnSO <sub>4</sub> ·7H <sub>2</sub> O	0.222
	Na <sub>2</sub> MoO <sub>4</sub> ·2H <sub>2</sub> O	0.39
	CuSO <sub>4</sub> ·5H <sub>2</sub> O	0.079
	Co(NO <sub>3</sub> ) <sub>2</sub> ·6H <sub>2</sub> O	0.049

■ Figures:

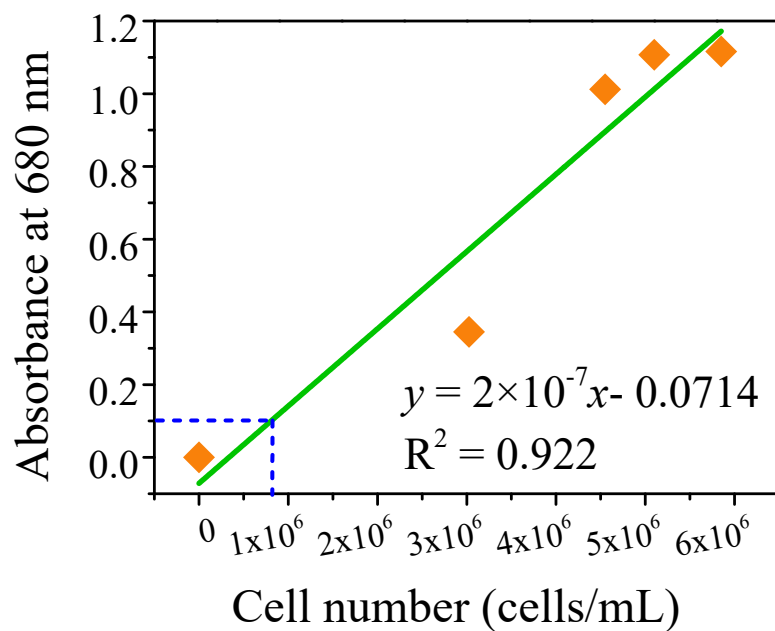


Fig. S1. The correlation between algal cell number and absorbance at 680 nm.

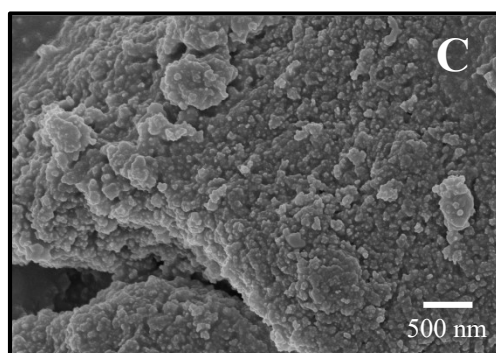
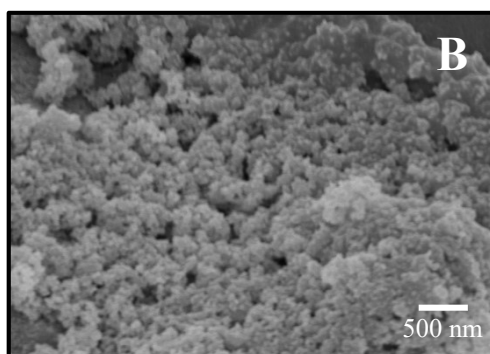
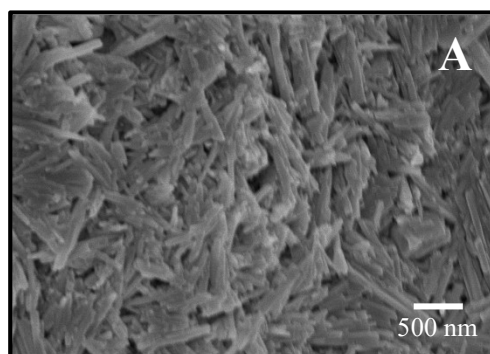


Fig. S2 The scan electron microscope (SEM) images of HNTs (A), nSiO<sub>2</sub> (B), and nAl<sub>2</sub>O<sub>3</sub> (C).

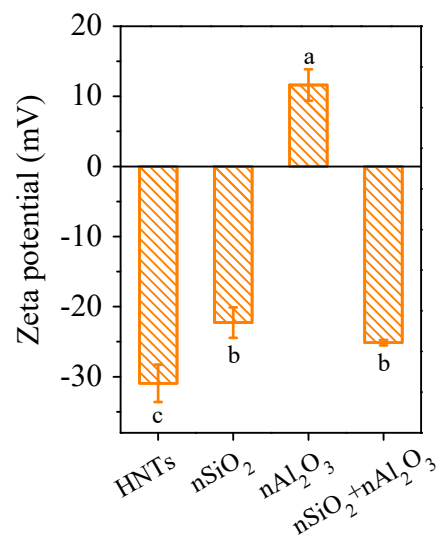


Fig. S3. The zeta potentials of tested nanomaterials in BG-11 medium.

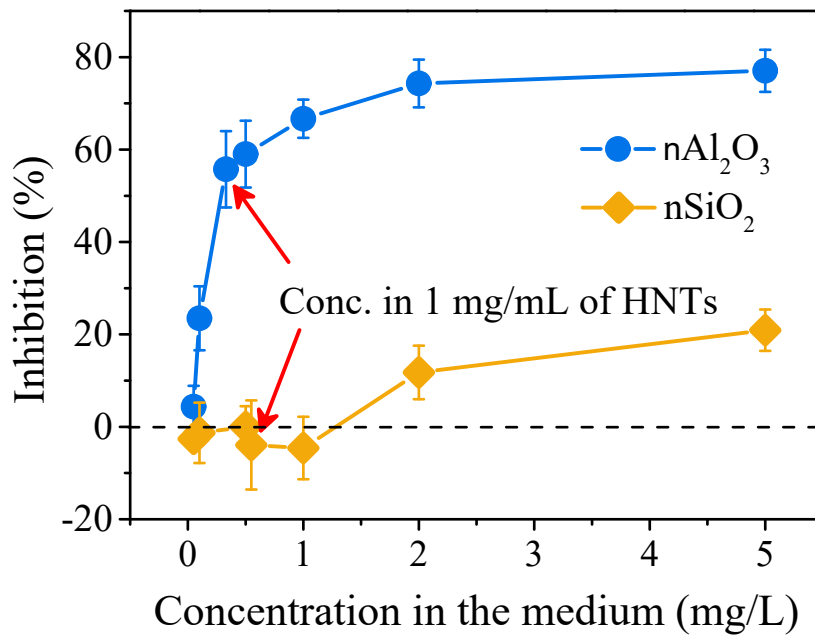
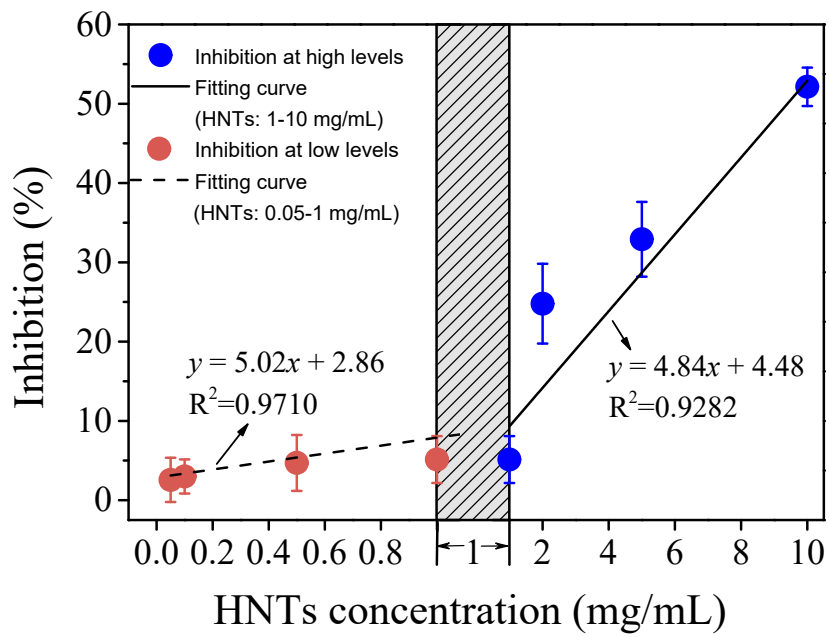


Fig. S4. The algal growth inhibition when exposed to different concentrations of HNTs,  $n\text{SiO}_2$ , and  $n\text{Al}_2\text{O}_3$ .

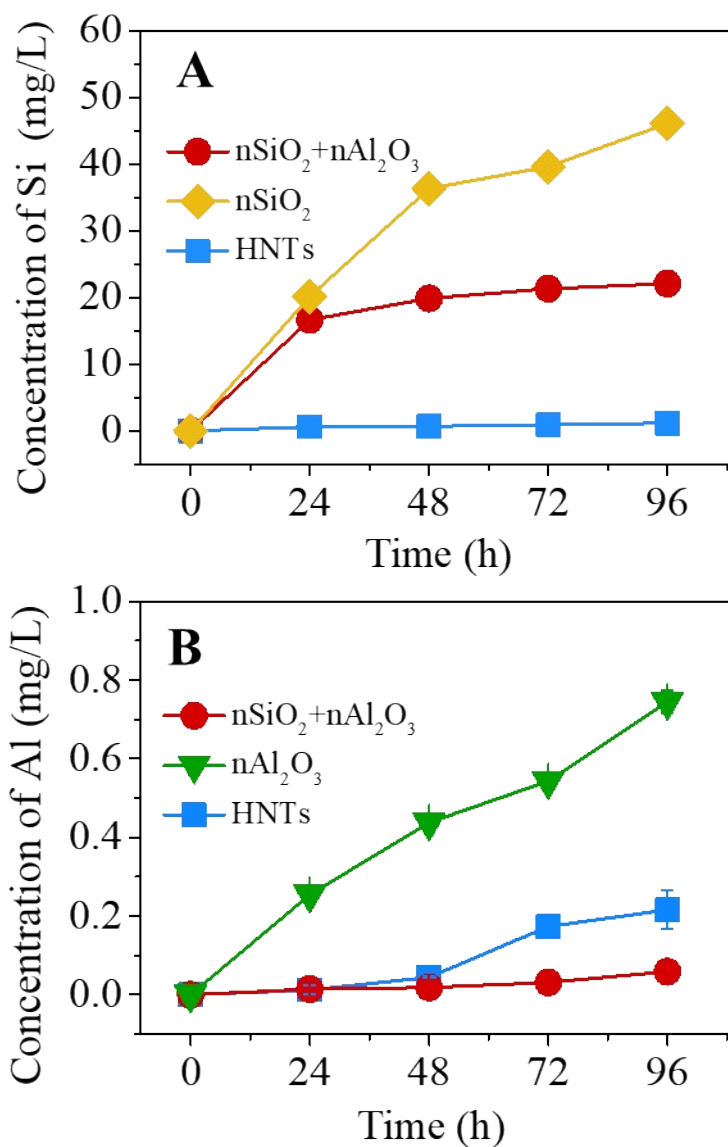


Fig. S5 The time-course of released Si (A) from HNTs, nSiO<sub>2</sub>, and nSiO<sub>2</sub>+nAl<sub>2</sub>O<sub>3</sub> and Al (B) from HNTs, nAl<sub>2</sub>O<sub>3</sub>, and nSiO<sub>2</sub>+nAl<sub>2</sub>O<sub>3</sub> in the algal medium.



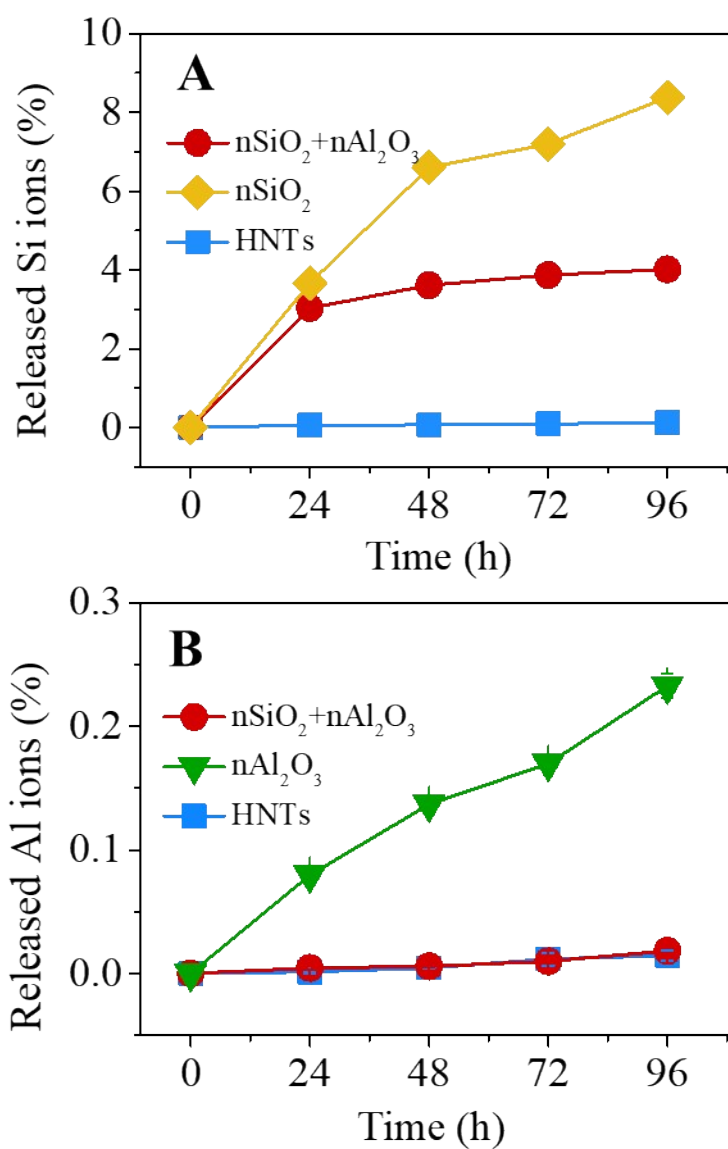


Fig. S6 The time-course of percentage of released Si (A) from HNTs, nSiO<sub>2</sub>, and nSiO<sub>2</sub>+nAl<sub>2</sub>O<sub>3</sub> and Al (B) from HNTs, nAl<sub>2</sub>O<sub>3</sub>, and nSiO<sub>2</sub>+nAl<sub>2</sub>O<sub>3</sub> in the algal medium.

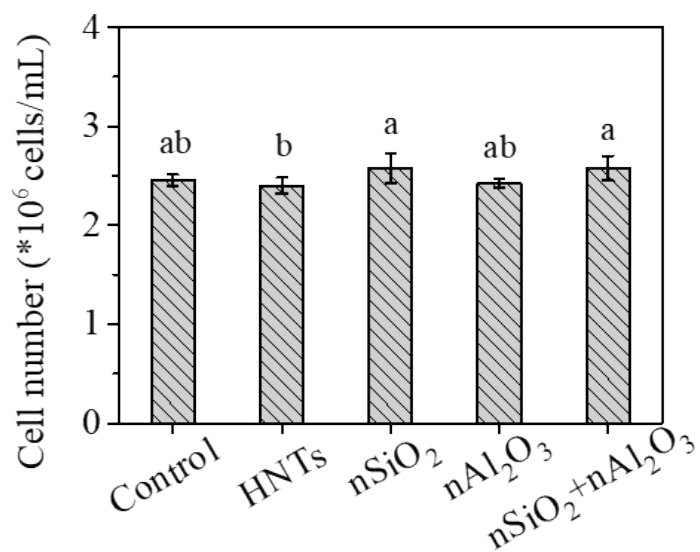


Fig. S7 The 96-h algal growth inhibition cultured under control and NMs-adsorbed medium. Lowercase letters represent significance in cell number among five treatments.

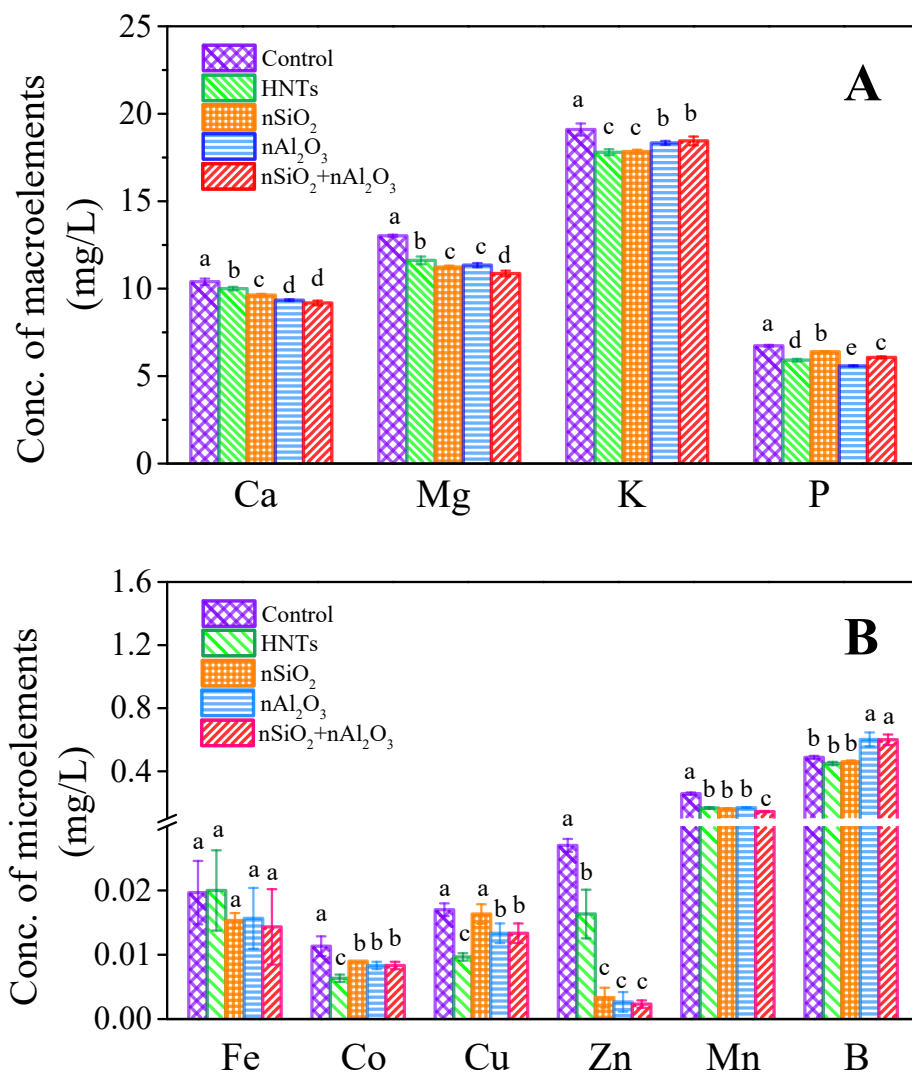


Fig. S8 Concentrations of macroelements (A) and microelements (B) in supernatants after adsorption for 96 h. Lowercase letters represent significance in macroelements and microelements among five treatments.

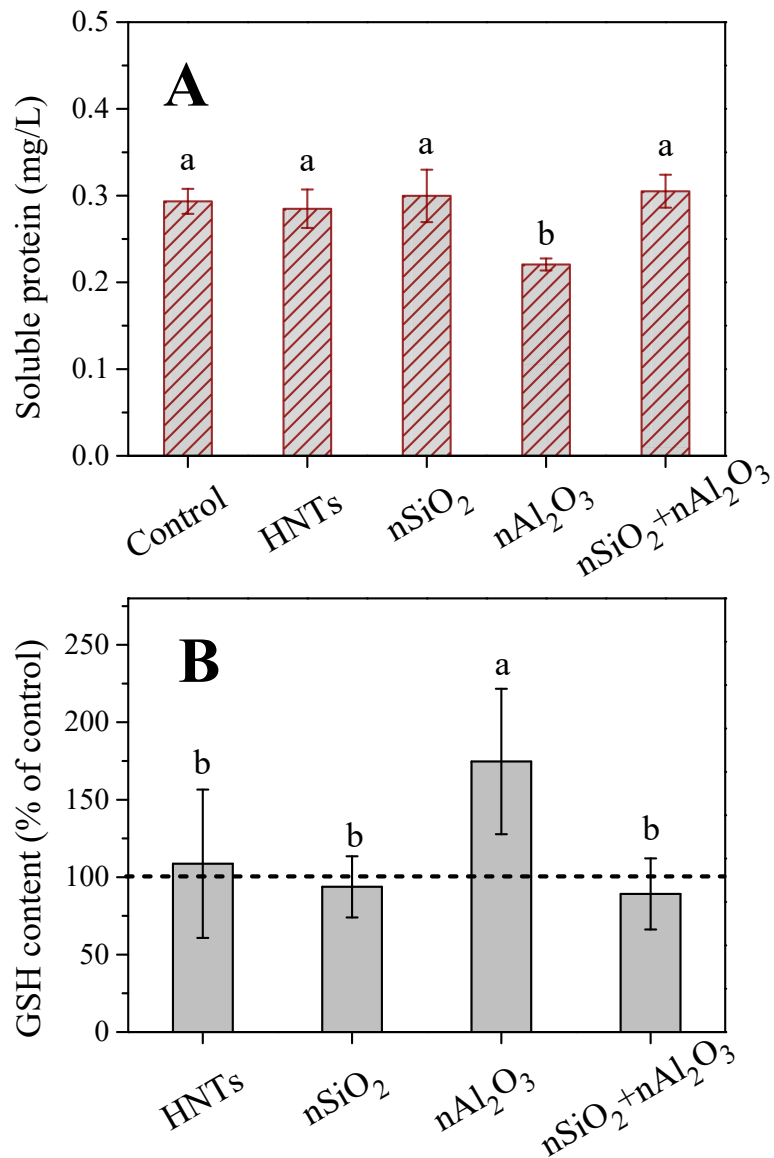


Fig. S9 The change of soluble protein (A) and GSH content (B) in algae under five treatments for 96 h. Lowercase letters represent significance in soluble protein and GSH content among five treatments.

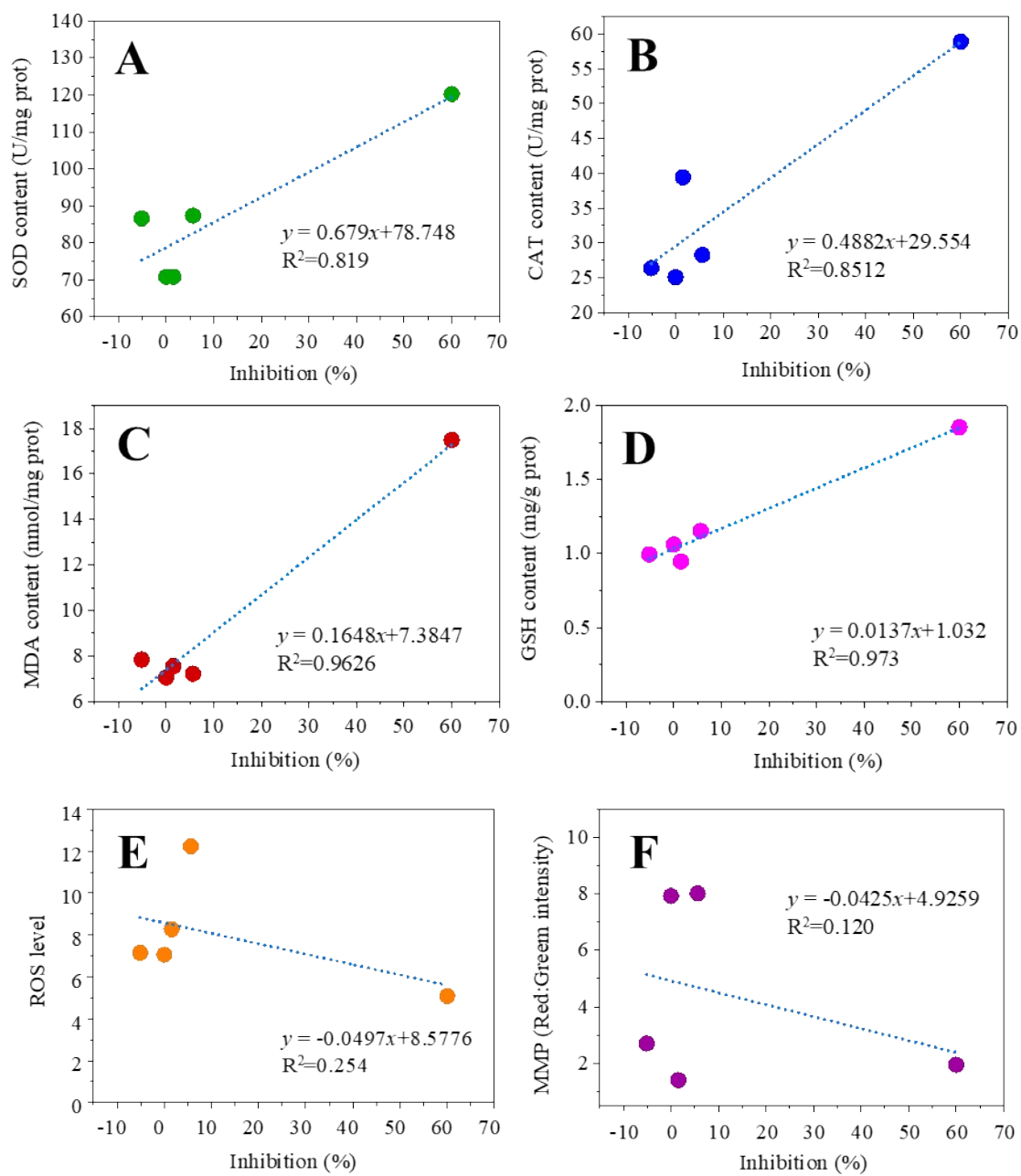


Fig. S10 The correlation between growth inhibition and SOD activity (A), CAT activity (B), MDA content (C), GSH content (D), ROS (E), and MMP (F).

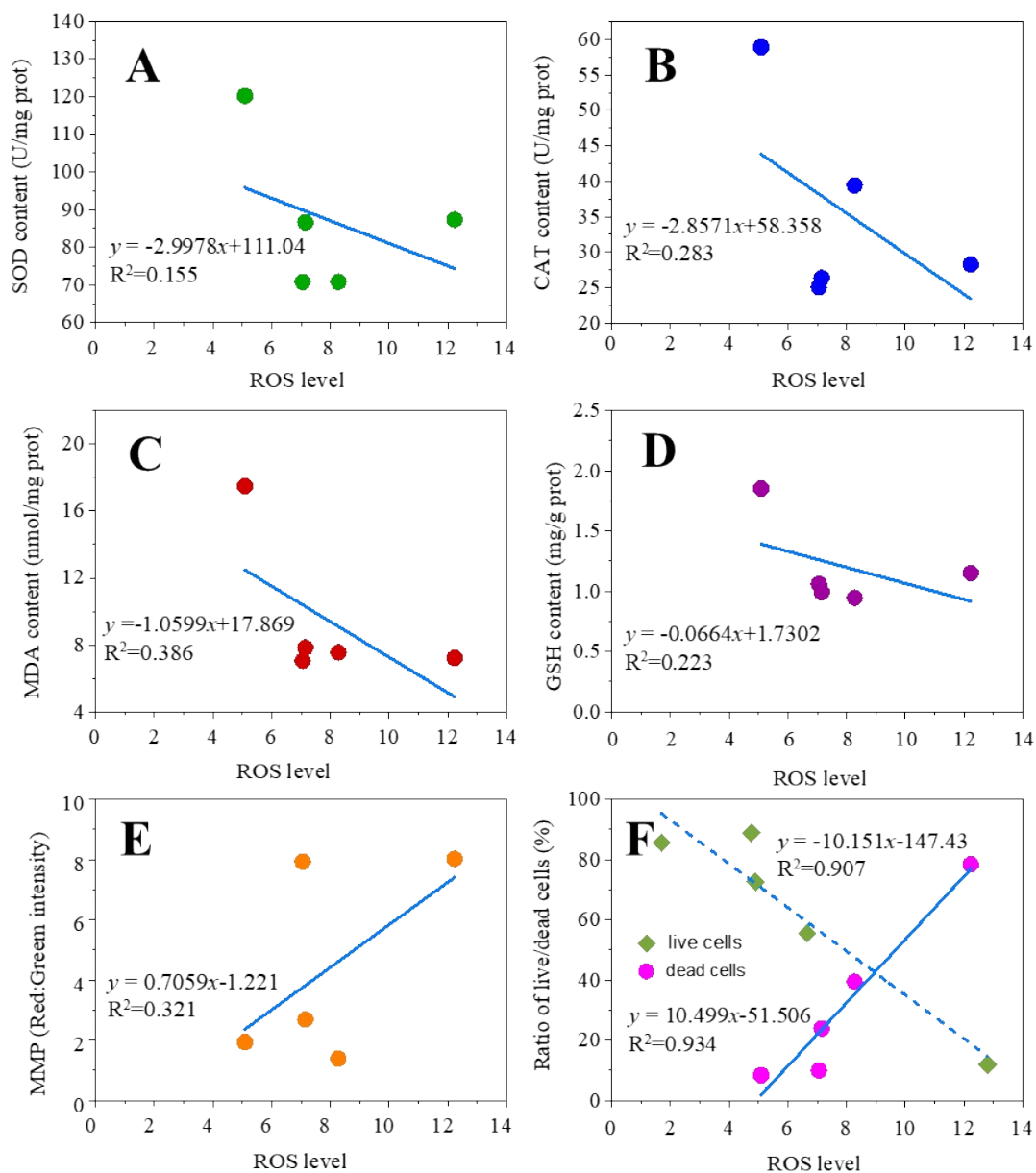


Fig. S11 The correlation between ROS level and SOD activity (A), CAT activity (B), MDA content (C), GSH content (D), MMP (E), and ratio of intact/injured cells (F).

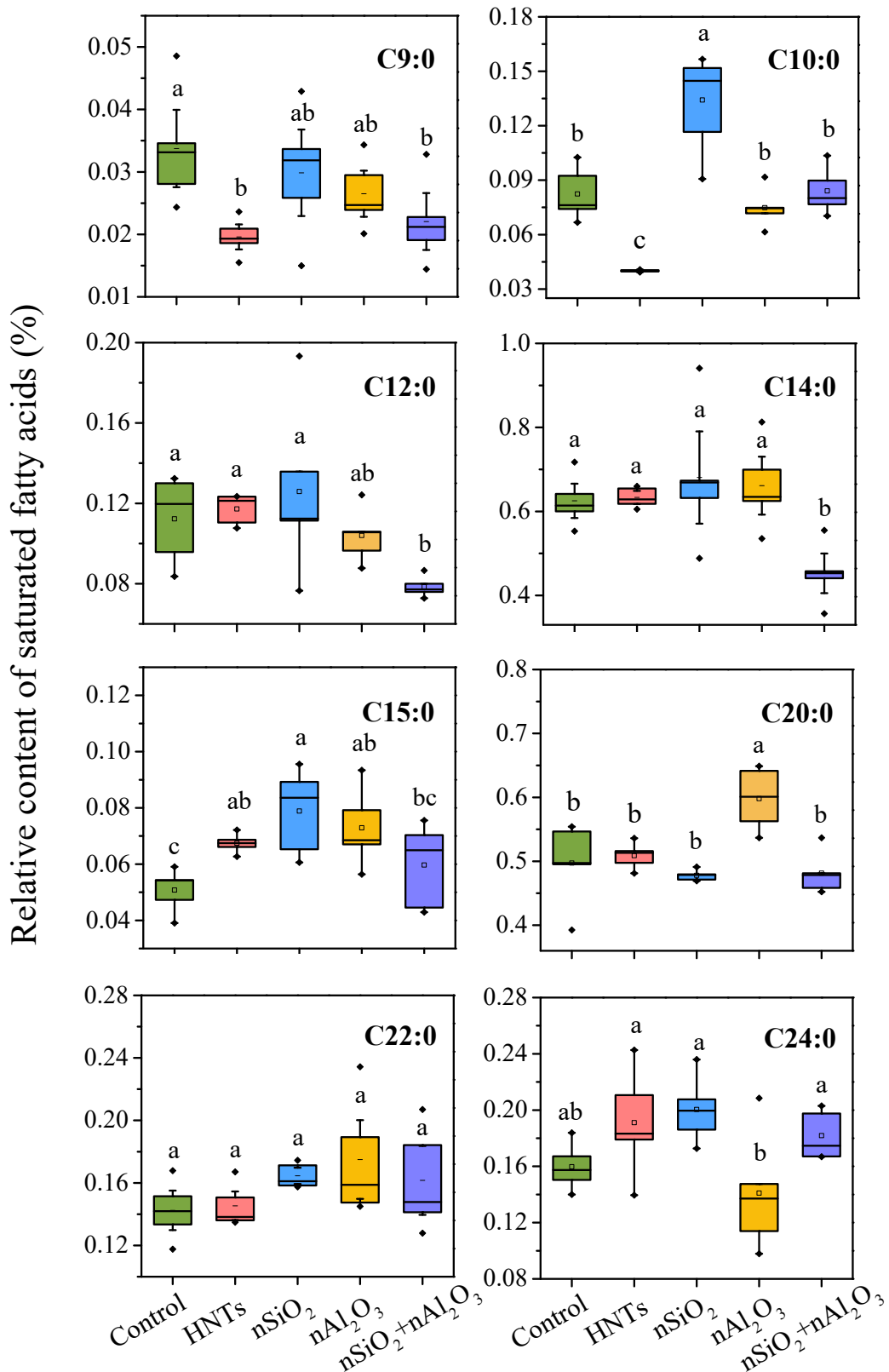


Fig. S12 The change of relative content (%) of several saturated fatty acids (SFAs) under HNTs, nSiO<sub>2</sub>, nAl<sub>2</sub>O<sub>3</sub>, and nSiO<sub>2</sub>+nAl<sub>2</sub>O<sub>3</sub> exposure. Lowercase letters represent significance in relative content of SFAs among five treatments.

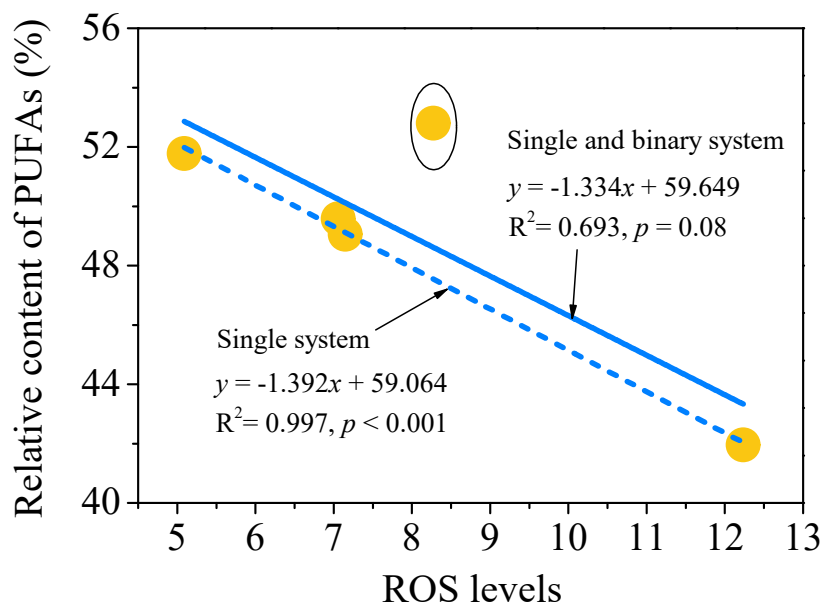


Fig. S13 The correlation between ROS and relative content of polyunsaturated fatty acids (PUFAs). The blue solid line and dash line represent linear fitting in the “single and binary” and “single” system, respectively.

*Note:* The difference in these two system is to fit with or without  $n\text{SiO}_2+n\text{Al}_2\text{O}_3$  mixture-related data.